KFA

KERNFORSCHUNGSANLAGE JÜLICH GmbH

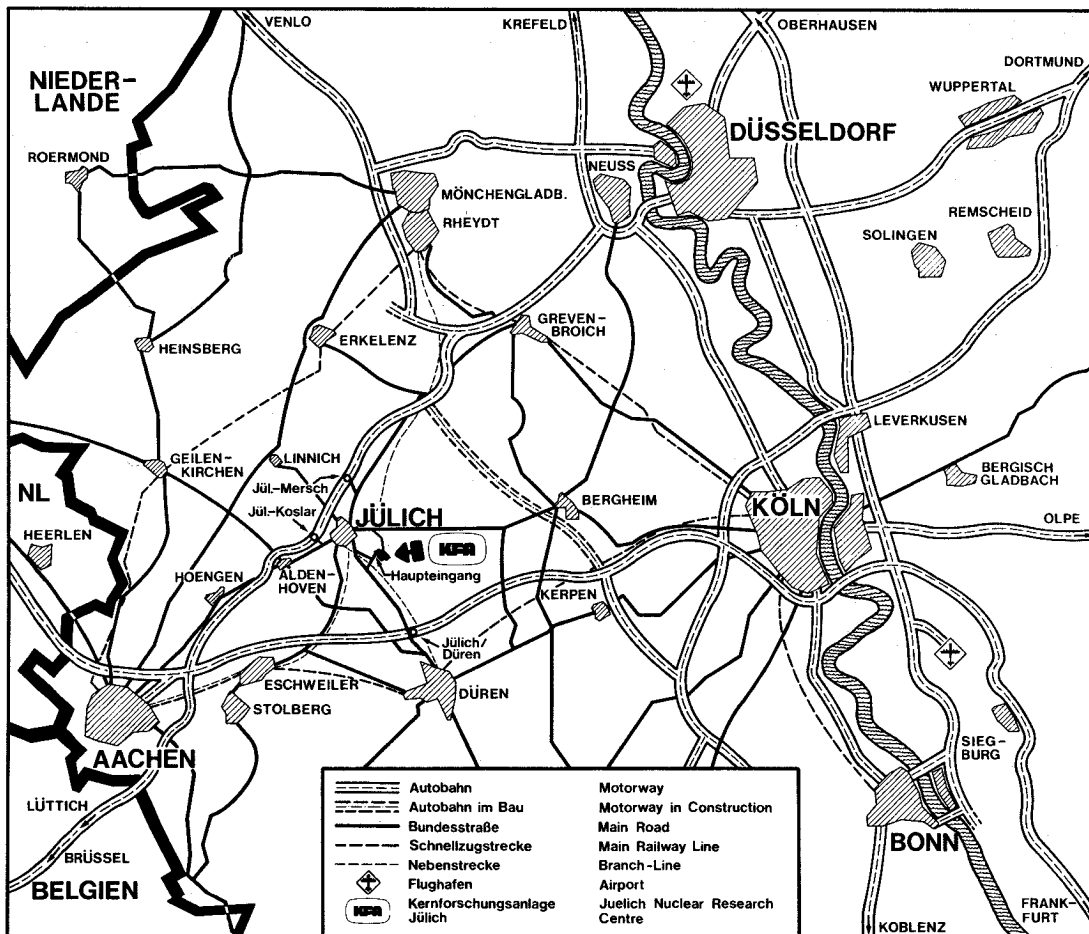Institut für Grenzflächenforschung
und Vakuumphysik

The Theory of Recoil Mixing in Solids

by

U. Littmark and W. O. Hofer

Map of the Jülich region showing motorways, roads, railway lines and the location of the Juelich Nuclear Research Centre (KFA). Legend:

Autobahn	Motorway
Autobahn im Bau	Motorway in Construction
Bundesstraße	Main Road
Schnellzugstrecke	Main Railway Line
Nebenstrecke	Branch-Line
Flughafen	Airport
Kernforschungsanlage Jülich	Juelich Nuclear Research Centre

The Theory of Recoil Mixing in Solids

Die Theorie der Stoßmischung in Festkörpern

U. Littmark and W. O. Hofer

Institut für Grenzflächenforschung und Vakuumphysik
der Kernforschungsanlage Jülich GmbH*, D-5170 Jülich,
Federal Republic of Germany

Abstract

In this review an attempt was made to describe the various physical models and theoretical approaches of collisional mixing in a unified notation based on standard theory of atomic collisions in amorphous solids. This allowes direct comparison of the respective underlying assumptions, the main regimes of validity, and an assesment of their relative accuracies. Owing to the variety of these models this unified description requires, however, a bulk of mathematical relations and expressions as well as symbols for physical and auxiliary quantities. Hence, in order to still serve as a readable review, this article is split into a more phenomenological review of recoil mixing, with a minimum of mathematics but containing all conlcusions from the second part, which is the presentation of existing models in a unified scheme. This part (Chap. 3 and 4), in turn, bases on the first one (Chap. 2) and is linked to it by multiple crossreferences. In addition, an introductory chapter intends to shed light into the jungle of terms and definitions currently in use, while a list of symbols refers to those quantities used throughout the article.

Particular emphasis was layed on in-depth concentration profiling by sputter-etching. This differs from the majority of recent work on ion-beam mixing in two respects: it is a low-energy (1-20keV) phenomenon, and it requires additional detailed knowledge on the transformation of internal concentration distributions into external (sputter-) profiles. Furthermore, the importance of determining the entire distribution functions instead of particular distribution parameters is stressed. Finally, the complications due to accumulation of ("reactive") projectiles in the target is addressed.

In diesem Übersichtsartikel wird der Versuch gemacht die verschiedenen physikalischen Modellvorstellungen und theoretischen Ansätze zur Stoßmischung in einem einheitlichen Schema, nämlich dem der Theorie atomarer Stöße in amorphen Festkörpern, zu beschreiben. Dies erlaubt einen direkten Vergleich der diversen Annahmen, ihrer Gültigkeitsbereiche und eine Abschätzung ihrer Genauigkeiten. Allerdings bedingt die Vielfalt der Modelle einen großen Aufwand mathematischer Beziehungen und Symbole für physikalische Größen. Um diesen Übersichtsbeitrag noch lesbar zu halten, wurde er in zwei Teile gespalten, und zwar in einen eher phänomenologischen Überblick über Stoßmischung, mit einem Minimum an Mathematik, doch alle Schlußfolgerungen des zweiten Teiles enthaltend. In diesem wird eine einheitliche Darstellung der Modelle gegeben; dieser zweite Teil basiert jedoch auf dem ersten und ist mit diesem durch zahlreiche Hinweise verbunden. Weiterhin wird in einem einleitenden Kapitel versucht in die Vielzahl der in Verwendung befindlichen Begriffe Klarheit zu bringen, und sind im Anhang in einer Liste alle diejenigen Symbole zusammengestellt, die in dem Beitrag durchgehend verwendet werden.

Besonderes Gewicht wurde auf die Stoßmischung bei der Anwendung der Zerstäubung zur Festkörper-Tiefenanalyse gelegt. Diese Art der Stoßmischung unterscheidet sich vom Großteil der neueren Arbeiten zur Ionenstrahlmischung in zweifacher Hinsicht: sie ist ein Niederenergie-Effekt (1 - 20 keV), und sie erfordert zusätzliche Information zur Transformation interner Konzentrationsprofile in (externe) Zerstäubungsprofile oder Oberflächenkonzentrationen. Auf die Wichtigkeit der Bestimmung der gesamten Verteilungsfunktion - anstatt einzelner Parameter - wird besonders eingegangen. Schließlich wird ein Problem diskutiert, das auftreten kann, wenn Projektilionen verwendet werden, die im Festkörper akkumuliert werden, wie dies bei Beschuß mit reaktiven Ionen der Fall ist.

Contents   Page

1. Introduction

The knowledge of the distortion of concentration profiles in solids
due to energetic particle bombardment is of vital importance in ion
beam analysis of solids, especially for concentration depth profiling
by sputter-etching. Controlled surface erosion by sputtering has be-
come such a powerful and universal technique, that even so serious
complications as beam-induced mixing have not impeded its expanding
range of applications. In fact, distortion of the original concen-
tration distribution due to energetic recoils generated by the probing
beam is _the_ inherent limitation of the method, after instrumental and
experimental complications have been eliminated. This becomes immediately
obvious when sputtering is realized as just one of the effects of recoil
generation and transport. Under typical depth-profiling conditions
only a minority of the generated recoils is emitted through the
surface, while 10-100 times more recoiling atoms are relocated in
the bulk. In multi-component targets these relocations may be ob-
servable, and the effect is generally referred to as recoil mixing.

Recoil mixing operates in all solids exposed to energetic particle
bombardment. The effect is most pronounced in concentration depth
profiling, although every effort is taken to minimize it. In sput-
ter depth profiling, the concentration analysis concerns the upmost
surface layers.Thus, in order to obtain a depth profile, all tracer
atoms have to be brought to the surface or vice versa. This means that sputter
depth profiling inevitably is a high fluence procedure, and that most analysed
atoms have experienced the entire cascade region. Moreover, not only

a tracer distribution, but also the matrix and the implanted
ion distribution will undergo alterations. There are for in-
stance pronounced differences in depth profiles obtained by
erosion with reactive ions and with inert gas ions, because
the latter are not collected in the target to any significant concentration
level. A special problem which has too often been disregarded
concerns, furthermore, the changes induced in the total target
density during high fluence bombardment.

Various attempts have been made to calculate the extent of com-
positional changes by recoil mixing /1-16/, since it cannot - as an
intrinsic effect - be circumvented by experimental skill or ex-
penditure. The prime aim of such theoretical attempts was, of course,
to obtain a *better understanding* of the underlying mechanisms. But
it was also realized, that results obtained even under highly sim-
plified conditions could be helpful for *unfolding experimental data*
in order to determine the original, genuine concentration distri-
butions. In this view, even random walk calculations of δ-function tra-
cers, to take an extreme example, appear to be justified.

Since recoil mixing assumes its full deployment in sputter depth pro-
filing, and since this method is also the central topic of this book,
most discussions in the following review are concerned with in-depth
concentration profiling by sputter etching. In chapter 2 we present a
gross overview of theoretical treatments of the phenomenon. As these
treatments cover very different approximations and approaches, a general
mathematical description of relocation phenomena is derived in chapter 3.
The formality of chapter 3, which is necessary for understanding the
various approximations applied to the problem, will be alleviated by
the specific evaluations given in chapter 4.

It, furthermore, constitutes the basis for forthcoming more general calculations.

1.1 Nomenclature

The two most prominent mixing process in sputter-depth profiling are

- *recoil mixing* due to the transfer of kinetic energy to target atoms, in elastic collisions and

- *radiation enhanced diffusion* due to migration of the additionally defects generated by the projectile and its ensuing secondary effects.

This review primarily deals with recoil mixing since this mechanism appears to be dominant at conditions under which depth analysis of solids usually is carried out.

Relocation of atoms by elastic collisions may happen either* by

- direct projectile-target atom interactions, in which case the process is termed *primary recoil mixing* /3-5/, or by

- high generations of recoils in the collision cascade, this being *cascade mixing* /6-16/.

Recoil mixing will of course always occur in ion beam analysis when the transferred kinetic energy exceeds the displacement threshold. It need not necessarily imply a higher degree of disorder in the target, although this will most often be the case. A prominent exception in this context is preferential sputtering, where enrichment of one component in the surface of an originally homogeneous multi-component target is often observed.

---

*This distinction between effets caused by primary- and cascade recoils is somewhat arbitrary. It represents the two extremes in the slowing down process for which theoretical models exist. Recent work on cascade evolution /31/ have partly filled the gap between these limiting cases.

We avoid the vague term *"atomic mixing"* /6/ for collisional mixing. It may, however, be used for description of the mixing phenomenon as a whole, hence including also migration and electrical drift effects.

The often used term *recoil implantation* concerns a special case of recoil mixing, the term "implantation" is meaningful only when mass transport across a defined plane or interface is considered /1-4/; it is, therefore, a typical low-fluence phenomenon. Recoil implantation may be due to either primary or cascade recoils. In the latter case it also works in the backward direction, i.e. mass and momentum transfer in the opposite direction than the incomming ion beam.

As a consequence of these different collision processes, widely differing depth resolutions were reported in the literature, ranging from the escape depth of sputtered ions ($\leqslant 5$ Å), to average cascade recoil ranges (10-15 Å), to average primary recoil ranges, up to the depth dimension of the cascade (typically 50-100 Å under usual analysis conditions).

2. Review of Recoil Mixing Models

There has been a long standing uncertainty as to the relative importance of primary and cascade recoils in recoil mixing /6,7-11/. Primary recoils, although fewer in number than cascade recoils, could well compensate this deficiency by virtue of their higher energy. Furthermore, cascade recoils would have energies hardly exceeding the displacement threshold E_d, and, for those which did, their approximately isotropic momentum distribution would result in just a symmetric broadening of the original profile. Hence especially the deeplying branch of the measured concentration profile could be markedly modified by long-range primaries. And indeed, the often observed asymmetric trailing of experimental depth profiles found interpretation in terms of primary recoil mixing.

There are however, two profound complications in such considerations: firstly, sputter depth profiling is not a static process involving low ($\lesssim 10^{14}$ cm^{-2}) projectile fluences Φ, but a continuous alteration of the concentration distribution in varying regions of the displacement cascade. Or, with reference to Fig. 1: even when starting with a δ-function like tracer profile $P(\Phi = 0, x)$ and having a bell-shaped distribution $P(d\Phi, x)$ after a fluence increment $d\Phi$, the next step will see a bell-shaped tracer profile exposed to a region with non-uniform recoil density. This will result in asymmetric tracer profiles even for perfectly isotropic recoil momentum distributions in the cascade. Moreover, even a symmetric bell-shaped internal profile will suffer asymmetric distortion during transition through the surface, see Sect. 3.3.1 and Fig. 3. Hence the appeareance of enhanced or prolonged tails in depth profiles is no proof at all for a dominating role of high energy primaries

with forward momentum distribution.

This momentum distribution of primary recoils is, on the other
hand, the second major complication in an assessment of their
role in recoil mixing. In addition, very little is known about
the variation of the momentum distribution in space. Only
for heavy projectiles in light targets ($M_1 > M_2$) can scattering
of the projectiles be neglected so that only forward knock-ons need to
be considered. Deviation from straight projectile trajectories,
which must be considered for the reversed case ($M_1 \leq M_2$) as well as at
deeper pentrations in the target, leads to material transport
also backwards, i.e. opposite to the beam direction.

2.1 Primary Recoil Implantation and Mixing

The term "implantation" as defined above refers to mass transport
across a certain well defined interface in the target /1 - 4/. Such
a situation exists only at the very beginning of the irradiation.
At fluences exceeding 10^{14}-10^{15} cm^{-2}, interface smearing has developed
to such a degree that transport of implanted material backwards into
the recoil "source" can no longer be neglected; the term "mixing" in-
stead of "implantation" is then more appropriate.

Let us consider a target, consisting of a substrate (atomic number Z_2,
mass M_2) and a surface layer (Z_3,M_3) of thickness D_3, bombarded with
ions (Z_1, M_1) having an incident energy E_1^o. If straight projectile tra-
jectories are assumed, i.e. scattering is neglected, implantation of
primary recoils is a straightforward problem. The depth distribution
of implanted surface layer atoms is then

$$\frac{dY_{PR}}{dx} = N_0 \int_0^{D_3} \int_{E_d}^{E_{3,max}} d\sigma_{13}(E_1(x'),E_3)F_{R3}(E_3,\cos\theta_3,x-x')dx' \qquad (2.1)$$

with

$$\cos\theta_3 = \sqrt{E_3/E_{3,max}} \quad , \quad E_{3,max} = \frac{4M_1M_3}{(M_1+M_3)^2} E_1 \equiv \gamma_{13}E_1 .$$

The scattering cross section $d\sigma_{13}$ is the probability for generating a primary M_3-recoil with kinetic energy E_3 by a projectile with energy E_1 at depth x'. F_{R3} is the range distribution of such primaries when generated with an angle θ_3 with respect to the surface normal. Integration extends over the transferred energy E_3 and the thickness of the recoil source D_3. This integral can easily be carried out for scattering cross sections derived from a power potential /17/ (first index: projectile, second index: target atom)

$$d\sigma_{ik}(E,T) = C_{ik} E^{-m_{ik}} T^{-1-m_{ik}} dT, \qquad o < m_{ik} < 1 \qquad (2.2)$$

and sharp recoil ranges /3 /

$$F_{R3} = \delta(x-\bar{R}_3) = \delta\left[x-3A_1^1 \cos\theta_3 \left(\frac{E_3^{2m_{32}}}{N_0C_{32}}\right)\right] \qquad (2.3)$$

where A_1^1 is a numerical constant /18/ and N_0 is the target density. For a thin recoil source, i.e. $D_3 < R_{3,max} = (\gamma_{13} E_1^o)^{2m_{32}} 3A_1^1/N_0C_{32}$ we obtain the depth differential recoil yield:

$$\frac{dY_{PR}}{dx} = \frac{N_0C_{13}}{(E_1^o)^{2m_{13}}} \frac{(R_{3,max})^\alpha}{m_{13}\gamma_{13}^{m_{13}}} \begin{cases} (x-D_3)^{-\alpha} - x^{-\alpha} & \text{for } D_3 < x < R_{3,max} \\ (x-D_3)^{-\alpha} - R_{3,max}^{-\alpha} & \text{for } R_{3,max} < x < R_{3,max} + D_3 \\ o & \text{for } R_{3,max} + D_3 < x \end{cases}$$

$$(2.4)$$

and the total primary recoil yield:

$$Y_{PR} = \int_{D_3}^{\infty} \frac{dY_{PR}}{dx} \, dx = \frac{N_0 C_{13}}{(E_1^o)^{2m_{13}}} \; \frac{D_3}{m_{13} \gamma_{13}^{m_{13}}} \; (\frac{1}{1-\alpha} \; (\frac{R_{3,max}}{D_3})^{\alpha} -1) \qquad (2.5)$$

with $\alpha = m_{13}/(2m_{32} + 1/2)$. For $m_{13} = m_{32} = 1/2$: $Y_{PR} \propto (D_3/E_1^o)^{2/3}$, similar to the result obtained by Moline et al. / 3 /.

A more realistic calculation takes projectile energy loss and range straggling of the recoils into account, for instance via a Gaussian recoil range distribution:

$$F_{R3} = \frac{1}{\sqrt{2\pi} \; \sigma_{R3}} \exp \; [- \frac{(x-\bar{R}_3)^2}{2\sigma_{R3}^2}]$$

$$\bar{R}_3 = 3 A_1^1 \cos\theta_3 \; \frac{E_3^{2m_{32}}}{N_0 C_{32}} \qquad (2.6)$$

$$\sigma_{R3}^2 = [A_0^2 + \frac{5}{2} A_2^2 \; (3 \cos\theta_3^2 - 1)] \; (\frac{E_3^{2m_{32}}}{N_0 C_{32}})^2 - \bar{R}_3^2$$

where A_1^1, A_0^2 and A_2^2 are constants evaluated in Ref. /18 /. The integrations must then be carried out numerically. Evaluation of this kind were presented in Ref. /9/ mainly for the sake of comparison with cascade implantation. This comparison clearly showed that cascade implantation is always the dominating part of both the total and the differential recoil implantation yield. Since the assumption of straight projectile trajectories strongly overestimates the yield, it can savely be concluded that the main mixing mechanism is due to cascade recoils.

2.2. Cascade Mixing

2.2.1 Random Walk Models

First analytical treatments of recoil mixing were based on a diffusion-like process /7,12-15/. This is essentially an approximation to the isotropic displacement cascade where the successive knock-on processes are described by random relocations over a small fixed step length. According to the solution of the diffusion equation with planar boundary conditions the smearing of an originally δ-function type transition within the time t is assumed to be transformed into a Gaussian distribution with standard deviation

$$\sigma = \sqrt{2\,D \cdot t} \qquad (2.7)$$

Similarly, a sharp interface (step-function type) transition will be transformed into an equivalent error function.

The diffusion coefficient D is related to the jump frequency Γ and the average jump distance (step length) $\bar{R}$ by

$$D = \frac{1}{6}\,\Gamma\,\bar{R}^2 \qquad (2.8)$$

An atom that is originally located deeper in the target than the depth extension of the cascade suffers an average total number of displacements before it reaches the surface and is sputtered, which is given by

$$\Gamma \cdot t = \frac{n_d}{Y} \qquad (2.9)$$

n_d is the number of displacements created within a collision cascade (due to one incident ion). For not too light projectiles the Kinchin-Pease formula can be used for n_d

$$n_d \cong 0.5 \frac{E_1^o}{E_d} \qquad (2.10)$$

Hence Eq.(2.7)gives

$$\sigma = \bar{R}\sqrt{\overline{n \cdot t/3}} = \bar{R}\sqrt{\frac{E_1^o}{6E_d Y}} \qquad (2.11)$$

Since the sputtering yield Y essentially follows the nuclear stopping power of the projectiles in the target, $\sim(E_1^o)^{1-2m_{12}}$ for a power potential, Eq. (2.2), the energy dependence of the broadening parameter σ is

$$\sigma \sim (E_1^o)^{m_{12}} \qquad (2.12)$$

The only free quantity in Eq.(2.11) is the average step length $\bar{R}$, which is of the order of 10 $\overset{o}{A}$. Hence σ can be evaluated in rather general terms.

This is basically the deduction and result of Andersen /7/. Although this way of treating cascade mixing was not new after the work of Haff and Switkovsky /12/, we have preferred this presentation here because the quantities used in /7/ are physically better defined and are, furthermore, based on the same assumptions of particle slowing down and energy deposition as used throught this work. This is the case also for Matteson's recent refinement of Eq.(2.8), which relates the diffusion coefficient to the deposited energy F_E and thus renders D depth-dependent,/14/ and chapter 3.3.1.

A short general discussion of cascade mixing calculations by random walk processes has been given by Carter /13/; according to this work doubts arise as to whether random walk criteria are fulfilled at all under sputter profiling conditions.

The simplifications of this kind of treating cascade mixing are obvious:

-the recoil cascade as well as the distorted profile are represented by a
single average quantity,

-the shape of the resulting profile is predetermined, thus profile shifts
and shape alterations are out of the range of application;

-the resulting profile concerns internal profiles only, not sputter-
profiles (see Sect. 3.3.1 and Fig. 1).

-injected projectile particles and their accumulation are disregarded.

In spite of these simplifications it is remarkable however, how well
the resulting relation for profile broadening sometimes agrees with
the experimental material /7/. Although the theory describes the
broadening of step functions only, it is conceivable that it can be used
for deconvolution of measured profiles - a procedure similar to un-
folding instrumental functions from experimental results.

In Chap. 3.1 it will be shown how diffusion equations can be obtained
from general transport theory. The restrictions required to achieve
such a simplification will then become   obvious. Specific solutions
of this approximation are presented in Chap. 4.2.1.

2.2.2 Transport-theoretical approach

The gradual alteration of a tracer density profile $P_3 (x,\Phi)$ with fluence Φ can
quite generally be described by a differential equation of the type

$$d(P_3(\Phi,x) \cdot \Delta x) = d\Phi \ \{ \int_0^\infty P_3(\Phi,x') \ \Delta x \ U_3(x',x) \ dx' -$$

$$- P_3(\Phi,x) \ \Delta x \int_{-\infty}^{+\infty} U_3(x,x') \ dx' \ \} \qquad (2.13)$$

where the (relative) relocation function $U_3(x,x')$ is defined by $P_3(x) \cdot U_3(x,x')$
dx dx' being the number of tracer atoms "3" displaced from the depth interval
(x,x+dx) to (x',x'+dx'). Equation (2.13) obviously consists of a loss term
due to recoils leaving the depth element under consideration, and a gain

term pertaining to recoils ending herein, see Fig. 1 for illustration.

The relocation function $U_3(x,x')$, which describes the displacement probability of 3-atoms, apparently depends on the actual target composition over the whole depth region covered by the collision cascade. This means that the balance equation (2.13) for multicomponenent systems is coupled to similar equations for the other target constituents, and thus is part of a _system of coupled nonlinear differential equations_.

Linearization of Eq.(2.13) can be obtained in two cases:

-if the collision dynamics of the components of the target is so similar
  that they can be regarded as one species (equal mass case), or

-if the concentration of the tracer component is so small compared to
  the matrix, that projectile slowing down and cascade evolution are
  essentially determined by the matrix (impurity-tracer case).

Decoupling, however, is only achieved in the first case. Equation (2.13) can then be solved independently.

If neither condition applies, the spatial distribution of the generation of one type of recoils depends on the instantaneous concentration distribution of all target constituents; no solution to this situation has been given as yet.

In order to solve Eq.(2.13) the relocation function $U_3(x,x')$ must be determined. Three ways of evaluating this function have been published so far: Ishitani and Shimizu /6/ determined it with the aid of their Monte Carlo simulation code.

Hofer and Littmark /8,9/ deduced it by using results from standard transport theory for multiple collision dynamics in random solids (recoil generation and recoil range).

Sigmund and Gras-Marti /10,11/ have, within the same theoretical scheme, set up a transport equation for $U_3(x,x')$. However, as their main interest seems

to be limited to shift and broardening of the density profiles
they avoided solving this transport equation, and determined only
the first moments over U_3. This theory therefore does not allow to
calculate the full distribution of tracer atoms and its alteration
with increasing fluence.

The procedure of determining the relocation function by computer-simulat-
ing recoil trajectories and sorting the recoils according to their pro-
jected range has repeatedly been published by Shimizu and coworkers /6/
at various grades of sophistication. Insertion of this function in
Eq.(2.13) then allows the calculation of both internal profile alteration
and "external" profiles, such as sputtered particle intensities (SIMS) or
surface concentrations (AES,ISS). The calculated profiles do show asym-
metries in the form of enhanced trailing tails, an effect which the authors
assumed to be due to primary recoils. Since, however, no variation of the
total target density during progressive irradiation was taken into account -
the importance of this effect was clearly recognized /6/ - and, further-
more, implanted projectiles were disregarded, this interpretation in terms
of primary recoils appears to be not quite secured. In this respect
Shimizu at al.'s calculations are still low fluence treatments.

This is also the case for the seemingly elegant treatment of Sigmund and
Gras-Marti /1o,11/, which invokes analogies with the Bothe-Landau
theory of energy losses. In addition to the neglect of density effects only
dilute tracer concentrations are considered, and implicitely it is assumed
that the probability for recoil-generation does not vary within the tracer
profile:

$$\sigma \cdot \frac{\partial}{\partial x'} U(x',x) \ll U(x',x) \qquad (2.14)$$

This results in rather simple relations for the profile shift and
broadening, and can well be related to random walk treatments /10/
(and sects. 3.3.1 and 4.2.1). In the light of the authors later
statement /11/,that shifts and broadenings are primarily due to
"high energy cascade recoils", assumption (2.14) appears to be in-
consistent.

Littmark and Hofer /8,9/ have presented a treatment which allows ar-
bitrary concentration profiles to be traced during high fluence bom-
bardment, _provided the mass of the particles involved are not too
different._ Apart from the assumption $M_2 \cong M_3$ this theory is rather
general, however. It allows accumulation of implanted projectiles,
gives a full description of the tracer profile alteration, and treats
the sputtering yield Y not as external input quantity determining the sur-
face erosion velocity, but as a quantity inherently coupled to the
collision cascade. Special features of this theory are discussed in
Chap. 4, in particular those which distinguish it from diffusion-like
treatments. An example demonstrating the capabilities of it is given at
the end of this review.

2.2.3 Miscellaneous Approaches

A rather extreme case of fast relocation under heavy particle bombardment has been discussed by Liau et al. /15/. Without specifying any physical mechanism these authors assumed complete equi-distribution over a distance L_c from the surface, which is smaller than the depth dimension of the collision cascade; the deeper-lying parts of the profile remain unaffected. In the notation of this review this reads

$$P(z,x) = \begin{cases} P(z,z) & z < x < L_c + z \\ P(o,x) & x > L_c + z \end{cases} \qquad (2.15)$$

where, we have used the position of the surface z instead of the fluence Φ as first variable. If sputtering is assumed to take place only from surface layers, the z/Φ-transformation is trivial

$$dz = \frac{Y}{N_o} \, d\Phi \qquad (2.16)$$

By observing particle conservation during continuous mixing and sputter-erosion, the balance equation in this particular situation reads

$$L_c \cdot P(z+dz, \, z+dz) = (L_c - dz) \cdot P(z,z) + dz \cdot P(o, z+L_c) \qquad (2.17)$$

or, in differential form

$$L_c \frac{dP(z,z)}{dz} = -P(z,z) + P(o, z+L_c) \qquad (2.18)$$

The solution of this differential equation can be given in closed form /15/. By taking moments over the genuine and the altered distributions, $P(o,x)$ and $P(z,z)$, - i.e. by multiplying Eq.(2.18) with z^n and integrating over z - one sees that the mean values (first moment) are identical whereas the

standard deviation (second moment) of the altered, "apparent" distribution increases with L_c

$$\sigma^2 (z) = \sigma^2 (o) + L_c^2 \qquad (2.19)$$

Thus, contrary to Eq.(2.11), equation (2.19) depends only on the cascade dimension but neither on the sputtering yield nor on the displacement threshold. Equations (2.11) and (2.19) share in common, however, the difficulty of dealing with a quantity which is supposed to represent a broad distribution function by a single, sharp value: $\bar{R}$ in Andersen's random walk description, and L_c in Liau et al.'s perfect profile-smearing. In one respect all these treatments come near to a result of more comprehensive theories: profile modification by energetic particle bombardment is very much determined by the dimensions of the collision cascade the projectiles generate. - This is also one of the results of a recent Monte Carlo calculation where recoil mixing is simulated directly, i.e. without determining first the relocation function and then the evolution of concentration profiles /16/. This way of a "forthright" determination of recoil dislocation will be discussed in Chap. 4.2.2.

Finally we should mention a quite different attempt to determine sputter-induced profile broadening, namely as a result of the stochastic nature of sputter-ejection of surface atoms /19/. In order to explain (static) SIMS signal intensities, such a model was originally proposed by Benninghoven /20/. It was based on the assumption that the probability for the ejection of a surface atom conforms to a Poisson-distribution, irrespective of whether or not neighbouring lattice sites are occupied. Hofmann and co-workers /19/ extrapolated this model (in various degrees of sophistication) to the field of in-depth profiling and suggested it was applicable for the evaluation of profile broadening and depth resolution. For a critical discussion of the experiments that were used to support this view we refer to Ref. 21; here we shall limit our comments to the physical basis for the model. Firstly, profile alteration is not simply a result of the development of surface structures with negligible influence from bulk recoil motion. Secondly, there is no evidence for steadily developing surface structures as indicated by the model; any known surface-morphology stabilizes during the doses necessary for depth profiling. Thirdly, although surface structures exert a deleterious effect on depth profiling, the effect itself is of less interest in so far as there are well known ways of minimizing it. This is for example not the case for the effects caused by recoil mixing.

3. General Formulation of Atomic Relocation Phenomena

In the preceeding review of the theoretical works on recoil mixing
it appears that the previous treatments cover several approaches.
We shall now try to derive a mathematical formalism within which
all these are contained. This should allow for a more detailed
comparison of the approaches, and for more insight in the approxi-
mations on which they are based. As it turns out that such a for-
malism is already rather complex, it does not involve much more
complication and labor to include also relocation effects which
are not of collisional origin. Although we shall only present re-
sults for the special cases of thermal and collisional relocations
(diffusion and recoil mixing), the aim of the following chapters
will be to give a general formulation of all possible atomic re-
locations taking place during ion bombardment of solids.

We consider bombardments with beams of ions characterized by their
atomic mass M_1, atomic number Z_1, energy E_1^o and direction $\bar{e}_1^o$. The
ion beam is so broad that lateral effects are inadequate. The spatial
description is then essentially one-dimensional and is performed in
terms of depths x measured perpendicular to the original plane surface.
The number of ions injected into the target is described through a
flux-density $\dot{\Phi}$ [ions/area/time] , which is constant over the bombarded
surface area but may vary with time. Φ is then the ion fluence [ions/
area] .

3.1. Target Description

The target consists of K atomic species with mass numbers M_k, and atomic numbers Z_k distributed in depth according to the density distributions $P_k(\Phi,x)$ [atoms/volume]. Target atoms of kind k which are set into motion are characterized by their energy E_k and direction of motion $\bar{e}_k$.

As Φ increases, all P_k functions change and then also the total target density:

$$N(\Phi,x)= \sum_{k=1}^{K} P_k(\Phi,x) \qquad (3.1)$$

changes. This involves a complication in the description (which has not always been realized). Usually the functions determining the atomic relocations (e.g. particle ranges) are evaluated under the assumption that N is constant. It is at present not possible in general to decide when a constant N is physically realistic. But as it is convenient to maintain this assumption, we introduce an auxiliary reference system, with depth scale y and concentration - distributions $Q_k(\Phi,y)$ so that

$$N_0 = N(\Phi=o,x)= \sum_{k=1}^{K} Q_k(\Phi,y) \qquad (3.2)$$

where N_0 is the original constant target density. The connection $P_k(\Phi,x) \leftrightarrow Q_k(\Phi,y)$ is given by simple local conservation of particle number in corresponding depth-intervals:

$$P_k(\Phi,x) \Delta x= Q_k(\Phi,y) \Delta y \qquad (3.3)$$

This transformation naturally conserves all local density ratios. The x-scale is considered as being stiff (independent of Φ), whereas the corresponding y-scale is varying due to the atomic relocations and (3.2). According to Eqs.(3.1-3.3) we get:

$$\Delta y = \frac{1}{N_0} N(\Phi,x) \, \Delta x \qquad (3.4)$$

and therefore

$$y(\Phi,x) = \frac{1}{N_0} \int_0^x N(\Phi,x') \, dx' \qquad (3.5)$$

The original x-scale _origo_ is kept during bombardment although the surface is continuously eroded away. In the P-system it is not possible to maintain a well defined surface position in general. The usual situation after prolonged bombardment appears to be that the total density gradually decreases to zero with decreasing depth (see Fig. 1 D). It is then a matter of definition where the surface is located. In the Q-system this difficulty does not exist: relaxation restores a constant total target density and thus a sharp surface located at y=0.

The interpretation of the Q-system is clearly (Eq.(3.5)) that it describes the real target in terms of a depth scale with areal density units [total no. of atoms/area]. In the following all profile changes caused by the ion bombardment will be described in the Q-system, and the evolution of the concentration profiles can be followed here. A general transformation $Q_k(\Phi,x) \to P_k(\Phi,x)$ can not be given as it involves the knowledge of the evolution of the total density $N(\Phi,x)$ during bombardment, and this may be rather different for different target complexes. However, as relative densities (concentrations) are identical in the two systems, the problem only consists in the establishment

of the correlation between Δy and Δx, or, in other words, in

defining a geometrical depth scale [e.g. in $\overset{\circ}{A}$-units]. We

shall illustrate the problem by two examples:

3.1.1 Unbounded Total Density $N(\Phi,x)$. (Fig. 1 D).

By "unbounded" we understand the situation that the total number

of atoms contained in a volume element is unrestricted. During

irradiation the number of particles in a (fixed) depth interval

Δx changes, whereas the number of atoms contained in the corres-

ponding Δy-interval is constant. Therefore Δy must change according

to (3.4). As the development of the individual Q_k functions can be

evaluated, however, the evolution of Δy can be followed for each

value of x, (Eqs.(3.2)-(3.4)).

We get then from Eqs. (3.3)-(3.5):

$$P_k(x) = Q_k \left(\int_0^x \frac{\Delta y(\Phi,x')}{\Delta x} \, dx' \right) \cdot \frac{\Delta y(\Phi,x)}{\Delta x} \tag{3.6}$$

which correlates the auxilliary Q_k-functions to the physical den-

sities P_k.

3.1.2 Total Density Bounded to $N(x) = N_0$. (Fig. 1 C)

Usually one imagines the physical target as obeying

$$N(x) = \begin{cases} 0 & \text{for } x < z \ (\Phi) \\ N_0 & \text{for } x > z \ (\Phi) \end{cases} \tag{3.7}$$

so that a sharp surface exist at depth $x = z(\Phi)$, determined by erosion, and with a constant internal total density, N_0 Eqs.(3.4-3.5) give in this case

$$\Delta y = \{ \begin{matrix} 0 & \text{for} & x < z \ (\Phi) \\ \Delta x & \text{for} & x > z \ (\Phi) \end{matrix}$$

$$y(\Phi,x) = \{ \begin{matrix} 0 & \text{for} & x < z \ (\Phi) \\ x - z(\Phi) & \text{for} & x > z \ (\Phi) \end{matrix} \tag{3.8}$$

(One might like to have the surface positioned at $x = 0$ which can be arrived at by a simple, but Φ dependent, coordinate transformation).

From (3.3) we obtain

$$P_k(\Phi,x) = \{ \begin{matrix} 0 & \text{for} \ x < z \ (\Phi) \\ Q_k(\Phi,x-z(\Phi)) & \text{for} \ x > z \ (\Phi) \end{matrix} \tag{3.9}$$

In Fig. 1 we have tried to illustrate these two systems together with the auxilliary Q-system. At low fluences (essentially $\Phi = 0$) the systems are identical (Fig. 1 A), but as Φ increases they show up rather differently.

The unbounded case 3.1.1 is, as hopefully evident from Fig. 1D, the most unrealistic one. We can document situations with steady state overdensities by a factor of 2. Also, the case 3.1.2 has limited applicability, namely to targets in which some sort of rapid relaxation towards total density N_0 is operating . Naturally the truth is somewhere between Fig. 1 C and Fig. 1 D, and if specific information on the bonds on $N(\Phi,x)$ is available, a combination of 3.1.1 and 3.1.2 can easily be used to obtain the correct values of $P_k(\Phi,x)$ from $Q_k(\Phi,y)$. For applications where a depth scale in atoms/cm² is sufficient, the $Q_k(\Phi,y)$-distributions themselves give the answer.

3.2. Description of Atomic Relocation.

In order to set up the equation describing the evolution of the concentration profiles Q_k during ion bombardment we need to define the relocation caused by one incident ion.

Let the absolute relocation function

$$V_k(E_1^\circ, \bar{e}_1^\circ, M_i, Z_i, Q_i, \Phi, \dot{\Phi}, y', y'')dy' \, dy'' \qquad (3.10)$$

$k, i = 1, \ldots, K$, be the number of k-atoms transferred from rest in the depth interval $[y', y'+dy']$ to rest in $[y'', y''+dy'']$ due to one incident ion $(M_1, Z_1, E_1^\circ, \bar{e}_1^\circ)$.

In (3.10) we have included all relevant dependencies. The dependence on Φ is usually implicit through the distribution functions $Q_i(\Phi, y)$ and the dependence on ion-flux $\dot{\Phi}$ is only relevant for high $\dot{\Phi}$-values. In the so-called linear cascade model, which may be considered as applicable in general, V_k is independent on $\dot{\Phi}$. V_k is made up of the probability for generating moving atoms at y', and the probability for transporting these from y' to y''. Therefore all y-values indeed enter V_k. As both these probabilities, however, are thought to be given by the target-configuration this dependence is again implicit through the $Q_i(\Phi, y)$-functions. The only explicit depth dependences are those of y' and y''.

In some interesting cases the probability for generating k-atoms at a depth y' is proportional to the number of k-atoms present at that depth, $Q_k(y')$. We can then write

$$V_k(y', y'') = Q_k(y')U_k(y', y'') \qquad (3.11)$$

where U_k has been named the relative relocation function (see sect. 2.2.2)

In order to explicitly indicate the aspects of generation and transport included in V_k we define

$$\frac{Q_k(y')}{N_0} \cdot F_{Vk} \ (E_1^\circ, \ \bar{e}_1^\circ, \ E_k, \ \bar{e}_k, \ y') \ dE_k \ d\bar{e}_k \ dy' \qquad (3.12)$$

as the number of k-atoms set into motion in the depth interval $[y', \ y' + dy']$ with energies in $[E_k, E_k + dE_k]$ and with directions in the solid angle element $d\bar{e}_k$ around direction $\bar{e}_k$ due to one incident ion $(E_1^\circ, \ \bar{e}_1^\circ)$ on the surface (y=o). F_{Vk} is the recoil velocity spectrum. Furthermore, we describe by

$$F_{Rk} \ (E_k, \ \bar{e}_k, \ y) \ dy \qquad (3.13)$$

the probability that such an atom is relocated over a depth-distance between y and y + dy, i.e. F_{Rk} is the range distribution for these atoms.

Later we shall study cases where the total number of moving atoms generated at depht y', the recoil intensity $I_k(E_1^\circ, \bar{e}_1^\circ, y')$, is varying with y', but where the normalized velocity spectrum $J_k \ (E_k, \bar{e}_k)$ is constant over the entire depht. In this situation the recoil velocity spectrum F_{Vk}, and consequently also the relocation funktion V_k, can be factorized

$$F_{Vk}(E_k, \bar{e}_k, y') = I_k(y') \ J_k(E_k, \bar{e}_k)$$

$$(3.15)$$

$$V_k(y', y'') = \frac{Q_k(y')}{N_0} \ I_k(y') \ \int_{E_k, \bar{e}_k} J_k(E_k, \bar{e}_k) \cdot F_{Rk}(E_k, \bar{e}_k, y'' - x') dE_k \ d\bar{e}_k$$

Eqs.(3.11-3.15) pretend that the generation and transport of atoms within the target can be determined for arbitrary configurations. This is a drastic overestimate of the present possibilities and severe approximations are usually necessary for evaluating actual V_k-functions. The energy pumped into the target by the ion beam or other external sources is first of all shared between the target constituents in a complex way which can hardly be determined even for a constant composition /22/. Evidently both the generation and transport of target atoms are further dependent on all concentration distributions over large regions in the target. These are steadily changing,so we necessarely deal with a complicated coupled and non-linear system. The proportionality between generation and presence of k-atoms at a certain depth, indicated by Eqs. (3.11-3.12), is fairly non-general, and F_{Vk} can usually not be taken as the generation in a pure k-target as tempted in Eq.(3.12).

After these pessimistic perspectives, it seems appropriate to indicate that there are indeed systems for which the input-quantities V_k can be evaluated. In targets where _all constituents have similar dynamic properties_ (practically identical atoms), F_{Vk} and F_{Rk} are independent of the concentration distributions and can be determined as for a pure target. The formulation Eq.(3.11-3.14) holds strictly true in this case. In targets where _one target constituent κ essentially dominates the dynamics_ of the target complex, V_k is only dependent on Q_k and Q_κ and evaluations seems again possible. Eq.(3.11) will not hold then, in the sense that U_k is independent on Q_k. For example for low energy recoil relocation, we could assume that energy deposition and particle slowing-down operate entirely in the κ-partial-system, and then by use of the energy sharing concept of Ref. /22/ arrive at recoil generation functions. These would in general be nonlinear in Q_k

though. If the dominance of κ is achieved due to *dominance of the density* Q_κ the problem would be even simpler and the formulation Eq.(3.11-3.14) again holds true. This last mentioned dilute-tracer-problem is the one which have been treated in Refs. /7,10,11 /. We shall return to this in section 4.2.

3.3. Ballance Equation for Atomic Relocation

During a fluence increment $d\Phi$, the number of k-atoms in an interval $[y,y+\Delta y]$ is changed by particles entering the interval and particles leaving it (see Fig. 1A). Thus the following balance equation must hold:

$$d(Q_k(\Phi,y)\cdot\Delta y) = \Delta y \, dQ_k(\Phi,y) + Q_k(\Phi,y) \, d(\Delta y)$$

$$= d\Phi \{ \int_{y'=0}^{\infty} V_k(y',y)dy'\Delta y - \int_{y''=-\infty}^{\infty} V_k(y,y'')dy''\Delta y + F_{RI}(y)\Delta y \, \delta_{1k}\} \quad (3.16)$$

where $F_{RI}(y)$ is the range distribution of the implanted ions, which for k=1 causes a source term in addition to the relocation. In the general description we include ion-implantation, although it may be neglected in many depth-profiling applications. This simplification is obtained by setting to zero quantities with index "I" in the following equations.

A few remarks must be made at this point: firstly, it must be remembered that Δy is changig during bombardment (in order to keep the total density constant); Secondly, we have in Eq. (3.16) - as it stands - artificially assumed the y"-values to cover the entire interval $[-\infty,\infty]$. Atoms ending up at negative y"-values are naturelly the sputtered atoms, and the total number of ejected k-atoms from $[y,y+\Delta y]$ per incident ion at fluence Φ is then:

$$S_k(\Phi,y) \, \Delta y = \int_{-\infty}^{0} V_k(y,y'') \, dy'' \, \Delta y \qquad (3.17)$$

and the k-atom partial sputtering yield is:

$$Y_k(\Phi) = \int_{y'=0}^{\infty} S_k(\Phi,y') \, dy' = \int_{y'=0}^{\infty} \int_{y''=-\infty}^{0} V_k(y',y'') dy' dy'' \qquad (3.18)$$

$V_k(y',y'')$ need not be known for negative y'' but then the corresponding part of (3.16) must be replaced by a given $S_k(\Phi,y)$-function. We are then dealing with a (real) semi-infinite equation (3.16).

Defining the effective total transfer function as

$$T_k(\Phi,y) = \int_{y'=0}^{\infty} [V_k(y',y) - V_k(y,y')] \, dy' \qquad (3.19)$$

We get for Eq.(3.16)

$$\Delta y \, d \, Q_k(\Phi,y) + Q_k(\Phi,y) \, d(\Delta y) =$$

$$d \, \Phi\{ T_k(\Phi,y) - S_k(\Phi,y) + \delta_{1k} F_{RI}(y) \} \, \Delta y \qquad (3.20)$$

Summation of (3.20) over k yields

$$d(\Delta y) = \Delta y \frac{d\Phi}{N_0} \{ T(\Phi,y) - S(\Phi,y) + F_{RI}(y) \} \qquad (3.21)$$

where $T = \Sigma T_k$ and $S = \Sigma S_k$

By insertion of (3.21) in (3.20) and by integrating (3.21) over Δy we finally arrive at

$$Q_k(\Phi + d\Phi, y + dy(\Phi,y)) = Q_k(\Phi,y) + dQ_k(\Phi,y)$$

with

$$dQ_k(\Phi,y) = \frac{d\Phi}{N_0} \{ N_0 [T_k(\Phi,y) - S_k(\Phi,y) + \delta_{1k} F_{RI}(y)]$$

$$- Q_k(\Phi,y) [T(\Phi,y) - S(\Phi,y) + F_{RI}(y)] \} \qquad (3.22)$$

and

$$dy(\Phi,y) = \frac{d\Phi}{N_0} \int_{y'=0}^{y} [T(\Phi,y') - S(\Phi,y') + F_{RI}(y')] \, dy'$$

where $dy(\Phi, y=0) \equiv 0$ so that the surface is always located at $y=0$.
Obviously we get

$$-dy(y=\infty) = \frac{d\Phi}{N_0} \int_{y'=0}^{\infty} [S(\Phi,y') - F_{RI}(y')] \, dy'$$

$$\qquad (3.23)$$

$$= \frac{d\Phi}{N_0} [Y(\Phi) - I_I(\Phi)]$$

where $Y = \Sigma Y_k$ is the total sputtering yield and I_I is the implantation
probability ($I_I = 1 - R_I$, where R_I is the reflection coefficient).
$-dy(y=\infty)$ is equal to the surface erosion dz caused by the fluence in-
crement $d\Phi$.

The changes in Q_k (Eq.(3.22)) are split up into two contributions: a direct change
(the first square bracket) and a change due to "relaxation" (the last square
bracket). The last part is then correlated to the change in y-position, dy.

As T_k and S_k are - through the V_k-function, Eqs.(3.17 3.19) - dependet
on all atomic density distributions (Q_i, i = 1...K), the evolution equa-
tions for the Q_k-distributions (3.22) consist of a complicated coupled
system of nonlinear equations. In order to allow analytical evaluation,
or to simplify numerical solution of Eq. (3.22) decoupling and/or a
linearization is desirable.

As long as the implanted ions are collected in the target, there is no way
to decouple or linearize the system. Decoupling is only possible in the
case of implantation in an originally pure target, a binary case: k=1,2.

This has been discussed in Ref. 23 but is of no further interest here.

Even in case that the implanted ions can be disregarded in the calculations, decoupling of the equations for just binary targets (matrix + tracer, $k = 2,3$) is in general impossible. A neccessary requirement is V_k to be independent of $Q_{i \neq k}$, but since the term $T = \Sigma T_i$ appears for all k this demand is not sufficient. Decoupling is possible only if:

(a) $V_k(y',y'')= Q_k(y') U(y',y'')$, i.e. if U_k(Eq.(3.11)) is independent on k, or if

(b)   the last square bracket in (3.22) can be considered as constant.

Whereas the last situation (b) can not be achieved without rather strange extra demands to the correlation between the relocation mechanisms for the different target species (see Sect. 3.3.1), the first case (a) can be realized for some important target systems: if all atomic species in the target posess similar collision dynamics, or if one atomic subsystem is entirely determining the slowing down process of primary projectiles and target atom recoils.

Case (b) has the pleasant property that $\frac{dy}{d\Phi}$ is constant, which makes it suitable for analytical treatments. Note that the equations need not be linear. An application of (a linearized version of) (b) will be given in sect. 3.3.1. (b) has been used in Refs. /10, 11   /.

Case (a)automatically linearizes Eq.(3.22)and this case will be treated in some detail in Sect.4.2.2. It has been used in Refs. / 8, 9   /.

If we return from the auxiliary Q-target to the real P-target we obtain in the unbounded target case (3.1.1):

$$P_k (\Phi+d\Phi,x)= P_k (\Phi,x) + d\Phi \left[T_k(\Phi,y)-S_k(\Phi,y) + \delta_{1k} F_{RI}(y) \right]$$

$$N (\Phi+d\Phi,x)= N(\Phi,x) + d\Phi \left[T(\Phi,y)-S(\Phi,y) + F_{RI}(y) \right] \qquad (3.24)$$

where

$$y (\Phi,y) = \frac{1}{N_0} \int_{x'=0}^{x} N(\Phi,x')dx'$$

and in the to $N(\Phi,x)= N_0$ bounded target (3.1.2) where $y= x-z(\Phi)$:

$$P_k (x,\Phi)= 0 \quad \text{for} \quad x < z (\Phi)$$

$$P_k (\Phi+d\Phi,x+dx(\Phi,x)= P_k(\Phi,x) +$$

$$\frac{d\Phi}{N_0} \{ N_0 \left[T_k(\Phi,x-z)-S_k(\Phi,x-z)+ \delta_{1k} F_{RI}(x-z) \right]$$

$$\qquad (3.25)$$

$$-P_k (\Phi,x) \left[T(\Phi,x-z)-S(\Phi,x-z)+ F_{RI}(x-z) \right] \} \quad \text{for} \quad x > z (\Phi)$$

with

$$d(x-z(\Phi))= dx(\Phi,x)-dz = \frac{d\Phi}{N_0} \int_{y'=0}^{x-z} \left[T(\Phi,y')-S(\Phi,y') + F_{RI}(y') \right] dy'$$

or with (3.23):

$$dx(\Phi,x)= - \frac{d\Phi}{N_0} \int_{x'=x}^{\infty} \left[T(\Phi,x'-z)-S(\Phi,x'-z) + F_{RI}(x'-z) \right] dx'$$

In both cases x is measured in the original (stiff) depth scale.

In order to evaluate (3.24) it is necessary to keep trace of $y(\Phi,x)$

during bombardment as the T- and S-functions are only known in the

Q-system.

Evaluation of Eq.(3.25) does not contain this complication because

the P- and Q-system only deviate in the depth scale with a (varying

but) known quantity, $z(\Phi)$.

3.3.1 The Diffusion Approximation

As mentioned in Chapter 1, the description of atomic relocation phenomena

as a diffusion-like process has been used extensively during the last years.

Here we present a diffusion approximation to the ballance equation 3.22 which

is applicable to collisional relocation as well as ordinary diffusion. In this

section the effects of the implanted ions will be neglected (quanitities with

Index "I" set equal to zero).

A diffusion approach is based on the assumption that _relocation distances_

are small compared to all dimensions otherwise entering the problem, e.g.

the width of the profile under consideration and the depth from which

atoms are transported to the surface, where they are finally registered.

This means that each atom considered has suffered many small relocations

before "detection". The general diffusion approximation then consists in a series

expansion of the balance equation in the small relocation length in order

to arrive at simpler equations. This expansion alone, however, does not

result in the linearization and decoupling of the balance equation, which

is (probably) necessary for solving the equations analytically. Sigmund

and Gras-Marti /10,11/ obtained linearization by assuming (implicitely)

that the target is bounded by zero total relocation $T(\Phi,x)=o$, and the

simplest sputtering process which just cuts away

a surface-layer of thickness $\frac{dz}{d\Phi}(\Phi)\ d\Phi = \frac{Y(\Phi)}{N_0}\ d\Phi$. The sputtering

yield $Y(\Phi)$ is an _external_ input quantity. In our notation this sputtering

is expressed as

$$d\Phi \cdot S_k(\Phi,y) = \begin{cases} Q_k(\Phi,y) \text{ for } y < \frac{dz}{d\Phi}\ d\Phi \\ \\ 0 \qquad \text{otherwise} \end{cases} \qquad (3.26)$$

and we then obtain

$$dx(\Phi,x) = 0 \qquad (3.27)$$

The bounded balance equation (3.25) with (3.19) and (3.11)

inserted then reduces to

$$\frac{\partial P_k(x)}{\partial \Phi} = T_k(\Phi,x-z) = \int_{x'=z}^{\infty} \left[P_k(x')U_k(x'-z,x-z) - P_k(x)U_k(x-z,x'-z) \right] dx' \qquad (3.28)$$

where $x = z(\Phi)$ is the position of the surface. Expansion of $P_k(x)$ to the

second order in $(x'-x)$ yields

$$-\frac{\partial P_k(x)}{\partial \Phi} = P_k(x) \int_{x'=z}^{\infty} \left[U_k(x'-z,x-z) - U_k(x-z,x'-z) \right] dx'$$

$$+ \frac{\partial P_k}{\partial x} \int_{x'=z}^{\infty} (x'-x)U_k(x'-z,x-z)\ dx'$$

$$+ \frac{1}{2}\ \frac{\partial^2 P_k}{\partial x^2} \int_{x'=z}^{\infty} (x'-x)^2\ U_k(x'-z,x-z)\ dx' \qquad (3.29)$$

Obviously, the assumption T=o, together with (3.26) fits into
the decoupling scheme (b) as presented in the previous section.
(The diffusion equation resulting from the scheme (a) is arrived
at by dropping the first term on the right hand side of Eq.(3.29).
So there is great similarity between the two diffusion equations;
but Eq.(3.27) is not valid in case (a), which makes (a) unsuitable
in the analytical diffusion approach).

As we now deal with a diffusion like process it is natural to try to
approximate P_k *with a Gaussian*. Using the eroded depth $z(\Phi)$ as variable
instead of Φ, we insert

$$P_k(z,x) = \frac{A_k(z)}{\sqrt{2\pi}\ \sigma_k(z)}\ \exp\left[-\ \frac{(x-a_k(z))^2}{2\ \sigma_k^2\ (z)}\right] \qquad (3.30)$$

and obtain for the parameters:

$$\ln \frac{A_k(z)}{A_k(o)} = \int_{z'=0}^{z} \frac{d\Phi}{dz}(z') \int_{x'=z'}^{\infty} \left[U_k(x'-z',x-z') - U_k(x-z',x'-z')\right] dx'dz'$$

$$a_k(z) - a_k(o) = \int_{z'=0}^{z} \frac{d\Phi}{dz}(z') \int_{x'=z'}^{\infty} (x'-x)\ U_k(x'-z',x-z')\ dx'dz'$$

$$\sigma_k^2(z) - \sigma_k^2(o) = \int_{z'=0}^{z} \frac{d\Phi}{dz}(z') \int_{x'=z'}^{\infty} (x'-x)^2\ U_k(x'-z',x-z')\ dx'dz' \qquad (3.31)$$

These formulae thus describe the evolution of a Gaussian k-tracer distri-
bution as a function of eroded depth z when the shape of the distribution
is prescribed as a Gaussian. Note, however, that the parameters are func-
tion of both x and z, so that the Gaussian approach can only approximate-
ly be maintained. Rigorously, the Gaussian approach is valid only if the
variation of U_k with generation-depth is negligible over the entire pro-
file for all relevant z-values, i.e. if

$$\frac{\partial}{\partial x^\prime} \, U_k(x^\prime - z, x - z) \cdot \sigma_k(z) \ll U_k(x^\prime - z, x - z) \qquad (3.32)$$

The inequality (3.32) is fulfilled as long as the profile remains narrow (low fluences) or the gradient in the relocation function is small (slowly varying relocation probability over the profile). For low energy collisional relocation or radiation enhanced diffusion, $F_{Vk}(x^\prime - z)$ — and therefore $U_k(x^\prime - z, x - z)$ — vary significantly with $x^\prime - z$, and at sufficiently high fluences (as necessary in depth profiling) the "diffusion" inevitably broadens the profiles so as to violate the inequality (3.32).

Provided, however, that (3.32) holds true, it is tempting to introduce the intensity/spectrum concept which led to Eq. (3.15), with $I_k(x^\prime - z) \cong I_k(x - z)$. Defining $\xi = x - x^\prime$ as the relocation length and $y = x - z^\prime$ as the actual depth below the surface we obtain from (3.31) with $Y(z) = N_0 \frac{dz}{d\Phi}(z)$

$$\ln \frac{A_k(z)}{A_k(0)} = \int_{y=x-z}^{x} \frac{I_k(y)}{Y(x-y)} \int_{E_k, \bar{e}_k} J_k(E_k, \bar{e}_k) \times$$

$$\times \int_{\xi=-\infty}^{y} \left[F_{Rk}(E_k, \bar{e}_k, \xi) - F_{Rk}(E_k, \bar{e}_k, -\xi) \right] d\xi \, dE_k \, d\bar{e}_k \, dy$$

$$a_k(z) - a_k(0) = \int_{y=x-z}^{x} \frac{I_k(y)}{Y(x-y)} \int_{E_k, \bar{e}_k} J_k(E_k, \bar{e}_k) \int_{\xi=-\infty}^{y} \xi \, F_{Rk}(E_k, \bar{e}_k, \xi) d\xi \, dE_k \, d\bar{e}_k \, dy$$

$$\sigma_k^2(z) - \sigma_k^2(0) = \int_{y=x-z}^{x} \frac{I_k(y)}{Y(x-y)} \int_{E_k, \bar{e}_k} J_k(E_k, \bar{e}_k) \int_{\xi=-\infty}^{y} \xi^2 F_{Rk}(E_k, \bar{e}_k, \xi) \, d\xi \, dE_k \, d\bar{e}_k \, dy$$

$$(3.33)$$

As long as the location ($\approx$y) of the profile is deeper than the relocation lengths, the three ξ-integrals in Eq. (3.33) reduce to: zero, the l_{mean} and the mean square relocation length, respectively. If, further, the velocity spectrum J_k is isotropic both $A_k(z)$ and $a_k(z)$ stay constant.

Especially simple is the situation where the relocation of tracer atoms can be described as a repeated isotropic stepping-process with a fixed steplength $\bar{R}$ (random walk). Under the above assumptions ($y \gg \bar{R}$), the erosion yield Y stays constant and we get

$$\sigma_k^2(z) - \sigma_k^2(o) = \frac{\bar{R}^2}{3Y} \int_{y=x-z}^{x} I_k(y) \, dy \qquad (3.34)$$

Identifying the integral as the total number of displacements in the depth-interval x-z to x in a pure k-target, equation (3.34) can be interpreted as justification of Eq.(2.11), /7/.

In case of a depth-independent "recoil" intensity function $I_k(y)$=const., for which normal thermal diffusion would be an example, the diffusion coefficient reads

$$D_k = \frac{\bar{R}^2}{6N_0} \dot{\Phi} I_k \qquad (3.35)$$

since the flux-density is $\dot{\Phi} = d\Phi/dt = N_0/Y \cdot dz/dt$.

Radiation enhanced diffusion or collisional relocation would operate with a depth dependent diffusion coefficient given by

$$D_k(x) = \frac{\bar{R}^2}{6N_o} \dot{\Phi} \; I_k \; (x-z) \tag{3.36}$$

It is tempting to investigate the approximations introduced to obtain Eq.(3.34) by solving directly the diffusion equation using (3.36). In terms of eroded depth it reads:

$$\frac{\partial P_k(z,x)}{\partial z} = \frac{\bar{R}^2}{6Y} \; \frac{\partial}{\partial x} \left(I_k \; (x-z) \; \frac{\partial P_k(z,x)}{\partial x} \right) \tag{3.37}$$

As we are interested in a qualitative comparison of the moments

$$P_k^n(z) = \int x^n \; P_k(z,x) \; dx \qquad n = 0,1,\dots \tag{3.38}$$

over P_k, we introduce the simple form

$$I_k(y) = \begin{cases} \frac{3C}{4R^3} \; (R^2-(y-m)^2) & \text{for } m-R<y<m+R \\ 0 & \text{otherwise} \end{cases} \tag{3.39}$$

which is symmetric around the maximum position at $y = m$. It approximates more sophisticated I_k's if the values of m and R are chosen to be the mean depth and $\sqrt{5}$ standard deviations of I_k, respectively. Equation (3.39) has the advantage that the moments can be found analytically from the recursion equation

$$\frac{2R}{n\alpha} \; \frac{\partial P_k^n}{\partial z} = - (n+1) \; P_k^n + 2 \; (z+m) \; P_k^{n-1} + (n-1) \; (R^2-(z+m)^2) \; P_k^{n-2} \tag{3.40}$$

with $\alpha = C\bar{R}^2/(4YR^2)$. For the mean tracer depth $a_k(z) = P_n^1/P_n^0$ we find for example

$$a_k(z) = (z+m - R/\alpha) + (a_k(o)-m+R/\alpha) \; e^{-\alpha z/R} \tag{3.41}$$

of for small z:

$$a_k(z)=a_k(o) - \frac{\alpha z}{R} (a_k(o) - m) \tag{3.42}$$

whereas the formalism (3.33) gave $a_k(z)=a_k(o)$.

According to (3.42) a tracer profile located at a negative gradient ($a_k(o)>m$) leads to a negative shift of a_k; this is due to stronger diffusion at regions $x<a_k$ than at $x>a_k$. For the same reason also a negative skewness is generated for this tracer location. The situation is naturally reversed for surface near tracer locations ($a_k(o)<m$) where the gradient is positive.

These results should be compared to the diffusion approximation to the balance equation, (3.30, 3.31), which gave no shift, $a_k(z)=a_k(o)$, and zero skewness.

The explanation for these discrepancies obviously is that the general diffusion equation (3.37) allows to take varying gradients in the relocation probability I_k into account, while the diffusion approximation to the balance equation implicitely ignores such gradients (3.32).

The solution to Eq. (3.40) is displayed in figure 2 for different values of α, together with the solution to (3.33). The parameter values are $m= 2/3 R$, $a_k(o)= 5/3 R$, $\sigma_k(o)= 1/20 R$ and skewness $(o)=o$, i.e. we start out with a narrow gaussian profile at the greatest depht where diffusion takes place. Obviously the profile does not stay gaussian (especially sensitive to the I_k-gradient is the skewness), and it is seen that the broadening resulting from the assumption underlying Eq. (3.33) yields an overestimate for large z, i.e. when the profile comes close to the surface.

Although both formalisms are invalid when the profile intersects the surface, there is a clear tendency for near-surface profiles towards a slightly positive skewness and a width that is comparable to the width of $I_k(y)$; note that the standard deviation of I_k is $R/\sqrt{5} \approx 0.45R$.

The conclusion of Fig. 2 is that the shape of the internal profiles is dramatically varying, so that the profiles need to be followed in detail during their evolution. A few parameters for the descripiton of, or, even worse, a pre-given shape of the profiles can lead to drastically erroneous results.

So far we have only treated internal profiles. The main interest for depth profiling purposes are however quantities like the surface concentration as a function of eroded depth $P_k(z,z)$. It has been the bad habit in previous diffusion treatments of this problem to identify moments over $P_k(z,z)$ with moments over $P_k(z,x)$, i.e. equalizing for example the standard deviation of $P_k(z,z)$ with $\sigma_k(z)$ as given by Eq. (3.33) with x=z inserted. Even if Eq. (3.33) were valid for internal profiles intersecting the surface (in an assumed infinite medium) the profile would develop during the passage of the fictive surface plane and the assumed internal-gaussian shape would <u>not</u> be transferred to the "external" $P_k(z,z)$ profile. In order to illustrate this problem we have inserted σ_k's resulting from different I_k's due to Eq. (3.34), with x=z, into Eq. (3.30). The original internal tracer profiles were δ-functions at depht $a_k=200$ Å and the mean number of relocations during erosion was fixed so as to yield the same standard deviation (80 Å) when penetrating the "surface": $\sigma_k=(z/a_k)^p \cdot 80$, where p results from different relocation mechanisms: p= $^1/2$ being representative for pure thermal diffusion and p= 1-2 for surface near radiation enhanced diffusion or collisional relocations. Fig. 3 present the resulting "external" profiles, i.e. the surface concentration

as a function of eroded depth. Although all internal profiles
are of gaussian shape the external ones exhibit long inward tails, the
stronger the larger p is. This extra
complication once more calls for evaluation of detailed profiles rather
than profile parameters, which might show up to be non-representative
for the problem /32/.

In the next chapter we shall go into more detail concerning the application
of the gaussian diffusion approach (3.33), but at this stage we should
draw   attention to the large number of approximations involved and
especially the one contained in $T(\Phi,x)=o$. It is unclear whether or when

the demand of a zero total relocation.

this assumption can be fulfilled. As far as the authors can judge, $T=o$
means that if atomic species of one kind are effectively removed from
a certain region, the deficiency is automatically cancelled by filling it
up with atoms of other types. Such a behaviour is fairly non-general, but
can be achieved if the generation of moving atoms is independent of depth
(e.g. if F_{Vk} is a constant) and all atoms are relocated similarly (e.g.
F_{Rk} is independent of k). This can be the case for usual thermal dif-
fusion. As soon as the generation varies with depth, or different atoms
have different relocation lengths (radiation enhanced diffusion and
collisional relocation), $T=o$ must be characterized as an unrealistic
approach.

Special attention should be drawn to the relation (3.32) which is a
necessary condition for the approach to be valid. Only narrow tracer dis-
tributions can be delt with and considerations on matrix-motion based on
Eq.(3.33) are misleading.

If the many assumptions contained in the development of Eq.(3.33) are partly or totally dropped, it is naturally still possible to apply the general diffusion approach, but little is gained then in simplicity as compared to the direct evaluation schemes which we shall return to in Section 4.2.2. For rough estimates the diffusion formulation, Eq.(3.33) might be sufficient and has as such been used by Haff and Switkowski /12/, Andersen /7/, and Sigmund and Gras-Marti /10,11/.

4. Solutions to the specific Mixing Models

In this chapter we shall use the general formalism developed in Chap. 3
in order to present the results of the main mixing models reviewed in
Chap. 2 in a unified notation and in some more detail.
The various approaches to atomic mixing are thus discussed as specific
solutions to the general balance equation for different relocation func-
tions. The main interest will lie, of course, with collisional reloca-
tion processes, especially with cascade mixing; we start out, however,
with thermally activated relocation processes, since they may always
contribute to concentration profile alterations in solids subjected to
energetic particle irradiation.

4.1. Thermal Mixing, Diffusion

This is plain diffusional deformation of concentration profiles due to random walk of dislodged atoms. In thermal diffusion both the concentration of point defects and their migration are in thermal equilibrium with the lattice. Radiation enhanced diffusion occurs when, due to the energetic particle bombardment, the concentration of interstitials and vacancies is increased. Diffusion is generally described by: _Per unit time there is a certain probability_ Γ, _that one atom is relocated isotropically a fixed distance_ $\bar{R}$. Γ is made up of the vacancy formation probability and migration probability which is determined by a Boltzmann factor: $\exp[-(E_f+E_m)/kT]$, where E_f, E_m and T are the formation energy, migration energy and temperature, respectively. In our formalism then the relocation length, angular spectrum and intensity is given by

$$F_{Rk}(\bar{e}_k,x) = \delta(x - \bar{R} \cdot \cos(\bar{e}_k, \bar{x}))$$

$$J_k = \frac{1}{4\pi}$$

$$I_k = \Gamma_0 \exp\left[-(E_f + E_m)/kT\right] N_0 / \frac{d\Phi}{dt} \qquad (4.1)$$

where $d\Phi/dt$ enters because I_k is defined per incident ion. The relocation distance $\bar{R}$ is of the order of the lattice unit. Since I_k is independent of depth, the diffusion approximation is valid, and, inserting Eq. (4.1) in Eq. (3.33), we find approximately $A_k(z) \cong A_k(o)$, $a_k(z) \cong a_k(o)$ and

$$\sigma_k^2(z) - \sigma_k^2(o) \cong \frac{\bar{R}^2}{3} \Gamma_0 \exp\left[-(E_f+E_m)/kT\right] \int_{z'=o}^{z} dz' / \frac{dz}{dt}(z') \qquad (4.2)$$

Identifying the integral as the diffusion time t, and recalling the solution to the classical diffusion equation: $D \cdot t = \Delta(\sigma^2)/2$, where D is the diffusion-coefficient, we have then obtained the Einstein relation $D = \bar{R}^2 \Gamma/6$.

For a constant flux-density $\frac{d\Phi}{dt} = \dot{\Phi}$ and sputtering yield Y, we obtain

for an original Gaussian k-atom-distribution: $[A_k(o), a_k(o), \sigma_k^2(o)]$ a

distorted "internal" distribution which stays Gaussian: $[A_k(o), a_k(o),$

$\sigma_k^2(o) + \alpha z]$, where

$$\alpha = \frac{N_o}{Y \cdot \dot{\Phi}} \frac{\bar{R}^2}{3} \Gamma_o \exp \left[- (E_f + E_m)/kT\right] \tag{4.3}$$

This is a consequence of the depth-independent relocation intensity I_k.
The apparent profile, i.e. the surface concentration as a function of
eroded depth then is

$$P_k(z,z) = \frac{A_k(o)}{\sqrt{2\pi(\sigma_k^2(o) + \alpha z)}} \exp \left[- \frac{(z - a_k(o))^2}{2(\sigma_k^2(o) + \alpha z)}\right] \tag{4.4}$$

It is important to note that this function may evince pronounced skewness
dependent on the magnitude of α. See Fig. 3.

Eqs. (4.1 - 4.4) are valid only for simple thermal diffusion. In case
of *radiation enhanced* diffusion the formation of vacancies
per ion is depth dependent and can be considered proportional to the so-
called deposited energy distribution $F_E(E_1^o, \bar{e}_1^o, y)$ /18/. The now depth-
dependent intensity function is

$$I_k(y) = I_k(x-z) = \left[\Gamma_o \exp(-E_f/kT)N_o/\dot{\Phi} + c_E F_E(x-z)/E_d\right] \cdot \exp(-E_m/kT) \tag{4.5}$$

where c_E is a well known constant /24/ and E_d is the effective displacement
energy. From (3.34) with x=z we get for a constant flux-density $\dot{\Phi}$ and a con-
stant yield Y

$$\sigma_k^2(z) - \sigma_k^2(o) \cong \frac{\bar{R}^2}{3Y} \exp(-E_m/kT) \times$$

$$\times \left[z \frac{N_o \Gamma_o}{\dot{\Phi}} \exp(-E_f/kT) + \frac{c_E}{E_d} \int_{y=o}^{z} F_E(y) \, dy\right] \tag{4.6}$$

Since F_E drops to zero at depths y larger than the ion range the contribution to broadening from radiation enhancement will be constant ($\int F_E(y)dy = E_1^o$) for original distributions lying deeper than the ion range. (However, referring to the discussion in Sect. 3.3.1, the diffusion approach (3.33) is not strictly valid in this case, and radiation enhanced diffusion should be treated in the approach, which will be presented in Sect. 4.2.2).

4.2 Recoil Mixing

In recoil mixing both *generation and motion* of dislodged atoms is treated as a consequence of collisional interactions. Rather detailed information can be derived from the literature on the relocation function V_k.

Especially simple is the treatment of *primary recoils* where the scheme of Eq.(3.14) can be used with

$$F_{Vk}(y) \, dE_k \, d\bar{e}_k = N_0 \, d\sigma_{1k}(E_1(y), \bar{e}_1(y), E_k, \bar{e}_k) , \qquad (4.7)$$

that is the cross section for generating a k-recoil ($E_k, \bar{e}_k$) when the projectile has energy and direction ($E_1, \bar{e}_1$). The latter quantities naturally depend on the preceding projectile history and therefore on the entire target configuration at the given stage. For light ions at low energies in a heavy target the velocity spectrum of the ions is approximately isotropic /25/, whereas $\bar{e}_1(y) = \bar{e}_1^o$ for the major part at the ion trajectory for high

energies or heavy ions in a light target. Then $E_1(y)$ is found
from

$$y = \int_0^{E_1(y)} dE'/S(E') \qquad (4.8)$$

where $S(E)$ is the projectile stopping power; the resulting velocity
spectrum of the k-recoils is usually strongly anisotropic (peaked
along the beam direction). This approach was used by Moline et al. /3/
to obtain results similar to Eq.(2.5), and by the present authors /9/ for
more detailed evaluations.

For *cascade recoils* one finds/24,26-28/ for a monatomic target

$$F_{Vk}(E_1^\circ, \bar{e}_1^\circ, E_k, \bar{e}_k, y) =$$

$$\frac{c_E}{4\pi} \frac{F_E(E_1^\circ, \bar{e}_1^\circ, y)}{E_k^2} + \frac{c_P}{4\pi} \frac{\bar{F}_P(E_1^\circ, \bar{e}_1^\circ, y) \cdot \bar{e}_k}{E_k^{3/2}} \qquad (4.9)$$

where $E_k \ll E_1^\circ$. c_E and c_P are numerical constants, and F_E and $\bar{F}_P$ are the
so-called deposited energy- and momentum depth distributions, respectively.
These have been evaluated on the basis of power cross sections in /18/ and
/28/. Using this procedure also for the determination of the range distri-
butions F_{Rk}, the entire U_k-function (Eqs.(3.11) and (3.14)) can be obtained
within a consistent scheme.

Equation(4.9) is essentially a series expansion of F_{Vk} in E_k/E_1°, the first
term representing a purely isotropic recoil velocity spectrum and the
second term the first anisotropies. In Ref. /9/ it has been
shown that the anisotropic terms as well as the few but high energetic
primary recoils have only minor effects on recoil relocation
in depth profiling contexts (see footnote on page 5). We shall therefore
concentrate at present

on the numerous low energetic cascade recoils, and

include then only the isotropic part of Eq. (4.9). It is well

established that these are the main contributors to sputtering

by heavy ions at keV-energies, and, as mentioned, also to almost

all profile disturbance during depth profiling by such ions.

is
As evident from Eq. (4.9), the intensity/spectrum concept of Eq.(3.15)

is applicable for low energy recoil generation in a mono-atomic target.

Within the presently available theories for recoil generation in multi-

component targets (and low energy recoils) we arrive at this conclusion

in general. Explicitly, if one tar-

get constituent, from now on arbitrarely called the matrix (label no. 2),

is entirely determining the dynamics in the target, i.e. energy deposi-

tion and recoil slowing down, then the matrix alone defines the energy

locally available for recoil generation, i.e. the depth dependence of

the generation probability for any kind of recoils I_k. This depth dependen-

ce is in general dependent of Φ, and must be evaluated for the ac-

tual matrix-subsystem: if we assume $F_E(y)$ to be known for a con-

stant (matrix) density N_o, we find the deposited energy at depth y for

$Q_2 \neq N_o$

$$F_E(Q_2,y) = F_E(E_1^\circ, \bar{e}_1^\circ, \frac{1}{N_o} \int_0^y Q_2(y')dy') \qquad (4.10)$$

The number of k-recoils generated at a certain depth y is further dependent on

the local concentrations and all atomic characteristics (M_i and Z_i), but

can be found by assuming that the energy sharing concept of Ref./22/ holds

locally:

$$F_{Vk}(y) = f_k(Q_i(y)) \frac{F_E(Q_2,y)}{4\pi E_k^2} \tag{4.11}$$

where $f_k(Q_i$, $i=1,...,k)$ are functions evaluated in Ref. /22/. The spectrum is then still an isotropic E^{-2} distribution. However, the k-recoil generation $\frac{Q_k}{N_0} F_{Vk}$ (Eq.(3.12)) is generally non-linear in Q_k (non-stoichiometric energy sharing).

The transfer-part F_{Rk} of V_k (Eq.(3.14)) must now be evaluated in a way similar to Eq.(4.10), so assuming both F_E and F_{Rk} to be given for a pure matrix-target with density N_0 we finally arrive at:

$$V_k(y',y) = \frac{Q_k(y')f_k(Q_i(y'))}{N_0} F_E \left(E_1^\circ, \bar{e}_1^\circ, \frac{1}{N_0} \int_0^{y'} Q_2(y'')dy'' \right) \times$$

$$\times \int \frac{1}{4\pi E_k^2} F_{Rk} \left(E_k, \bar{e}_k, \frac{1}{N_0} \int_{y'}^{y} Q_2(y'')dy'' \right) dE_k \, d\bar{e}_k \tag{4.12}$$

In case that the matrix dominance is achieved by an *overall density dominance* ($Q_2 \cong N_0 \gg Q_{k \neq 2}$, the "dilute tracer" case), Eq.(4.12) is especially simple. We get from Ref./22/ that:

$$f_k = \gamma_{2k}^{1-m} \frac{C_{2k}}{C_{22}} c_E \tag{4.13}$$

where $\gamma_{ik} = 4M_i M_k/((M_i+M_k)^2)$ and C_{ik} are the mass and atomic number dependent constants in the applied power cross section (2.2), where the same $m_{ik} = m$ has been assumed. Eq.(4.12) now reduces to:

$$V_k(y',y) = \frac{Q_k(y')}{N_0} \left[\gamma_{2k}^{1-m} \frac{C_{2k}}{C_{22}} \right] c_E F_E (E_1^\circ, \bar{e}_1^\circ, y') \times$$

$$\times \int \frac{1}{4\pi E_k^2} F_{Rk} (E_k, \bar{e}_k, y-y') dE_k \, d\bar{e}_k \tag{4.14}$$

This dilute tracer model is the one used in Refs. /10,11/,

where *additionally the diffusion approach* was applied.

In case that *all target constituents are dynamically identical,* no
restrictions need to be made for the magnitude of the densities, and we
again get a simple expression:

$$V_k(y',y) = \frac{Q_k(y')}{N_o} \; c_E \; F_E \; (E_1^\circ, \; \bar{e}_1^\circ, \; y') \; \times$$

$$\times \int \frac{1}{4\pi \; E_k^2} \; F_{Rk}(E_k, \; \bar{e}_k, \; y-y') \; dE_k \; d\bar{e}_k \qquad (4.15)$$

where F_{Rk} is the—now k-independent—recoil range. Eq. (4.15) is contained in
Eq. (4.14) as the factor in the square bracket reduces to unity in this "equal
mass" case. The above approach was the one used in Refs. /8,9/.

In specific evaluations of the functions F_E and F_{Rk} from transport theory
by use of power cross sections (2.2) the power parameter m_{ik} has to be
chosen with care: in the deposited energy function F_E the projectile - target -
atom interaction is essential (1 → 2), while only collisions between target
atoms (k → 2) enter F_{Rk}; the "high-energy" m_{12} used for F_E determination is
therefore generally larger than the m_{k2} applied to the low energy F_{Rk} eva-
luation.

In the following we shall concentrate on the dilute tracer case and the
equal mass case, and we shall use for both the notation Eq.(4.14), though
remembering the density-restriction when the square bracket is *not* unity.

4.2.1 Cascade Mixing, Diffusion Approaches

Since sputtered atoms are generated relatively close to the surface (~ 10 Å) while the cascade dimensions are much larger, we could, as a first estimate of collisional relocations, turn once again to the diffusion approach. Of course all the necessary reservations, namely that we deal with a dilute and narrow tracer, still apply.

Inserting (4.14) in Eq. (3.33) with x=z results in

$$\sigma_k^2(z) - \sigma_k^2(o) \cong \left[\gamma_{2k}^{1-m} \frac{C_{2k}}{C_{22}} \right] c_E \int_{y=0}^{z} \frac{F_E(y)}{Y(z-y)} \int_{E_k, \bar{e}_k} \frac{\xi^2}{4\pi E_k^2} F_{Rk}(E_k, \bar{e}_k, \xi) \, d\xi dE_k d\bar{e}_k dy$$

(4.16)

If we approximate F_{Rk} with a δ-function around a fixed $\bar{R}_k$ (as in the treatment of thermal relocation) we obtain for a Gaussian profile, originally positioned deeper than the ion range, and for a constant sputtering yield Y:

$$\sigma_k^2(z) - \sigma_k^2(o) \cong \left[\gamma_{2k}^{1-m} \frac{C_{2k}}{C_{22}} \right] c_E \frac{E_1^o}{E_d} \frac{\bar{R}_k^2}{3Y}$$

(4.17)

This result is almost the same as the term arising from radiation enhancement in thermal diffusion (Eq. 4.6), apart from the missing migration probability. The average step length $\bar{R}_k$ is much larger here since it is determined by collisions (~ 10 Å). Eq. (4.17) is identical to Eq. (2.11) in the equal mass case as $c_E \cong 0.5$ /23/.

For a more realistic recoil range distribution, evaluated via power cross sections (Eq. (2.6)), we find under the same conditions as used for ob-

taining Eq. (4.17), and for $m_{k2} < 1/4$ and $E_1^o \gg E_d$:

$$\sigma_k^2(z) - \sigma_k^2(o) \cong \left[\gamma_{2k}^{1-m} \frac{C_{2k}}{C_{22}}\right] c_E \frac{E_1^o}{E_d} \frac{1}{\gamma} \frac{A_o^2}{1-4m_{k2}} \left(\frac{E_d}{N_o C_{k2}}^{2m_{k2}}\right)^2 \qquad (4.18)$$

just a modified version of (4.17), which, however, does not contain any

free variable. (A_o^2 is a numerical constant /18/).

Eqs. (4.17) and (4.18) were originally derived in Ref./7/ and /10/. They seem to be

suitable for qualitative estimates of internal profile-broadening, since

as all quantities entering Eq. 4.18 are relatively well known.

Gras-Marti and Sigmund /11/ tried to avoid the splitting up of U_k in F_{Vk}

and F_{Rk} (Eqs. (3.11) and (3.14)) by writing down directly the transport

equation for U_k in the dilute tracer model. They, however, did not solve

this equation but dumped it into the diffusion approach.

The common feature of all previously mentioned diffusion approaches is

that their results are rather questionable under depth profiling condi-
tions. With reference to the discussion of the diffusion approach in Sect.3.3.1,

at least σ_k must be demanded to be much smaller than the dimen-

sions of the collision cascade. Inserting realistic values for γ, A_o^2 and

c_E (~ 0.5) we need cascade dimensions much larger than 50 Å, where much

larger means that the driving "force" F_E *must not fluctuate* within this

distance. Under usual depth profiling conditions ($E_1^o \lesssim 20$ keV heavy ions)

it is obvious that this basic assumption cannot be fulfilled. As noticed

by Carter /13/ this implies that rapid multi-relocation ("diffusion") is quickly bringing relocated atoms to the boundaries of the cascade. Therefore the profile broadening σ_k is determined by the cascade dimensions rather than by the quantities given by Eqs. (4.17) and (4.18). See also Fig. 2.

A model for extremely rapid relocation, namely a uniform smearing out of any concentration gradient within a characteristic cascade depth L_c, was proposed by Liau et al. /15/ and discussed in Sect. 2.2.1. This model cannot be incorporated into the above scheme because the relocation mechanism is unspecified. However, the (trivial) conclusion in the present notation is that the broadening is given as

$$\sigma_k^2(z) - \sigma_k^2(0) = L_c^2 \qquad (4.19)$$

i.e. defined by the cascade dimension $L_c(M_i, E_1^0)$. (Incidentially, in this case of rapid "diffusion", the assumption $T = 0$ is obviously valid.) It is furthermore noticed that it represents an extreme case of Carter's statement.

The "rapid diffusion" model, Eq. (4.19), and the "slow diffusion" model, Eq. (4.18), obviously represent the two extreemes concerning the speed of relocation of bulk atoms relative to the speed of removal of surface atoms. These speeds are more or less the ad hoc basis for these approaches. In order to avoid such pre-given assumptions in the calculation of cascade recoil relocation one should return to the original balance equation (3.22) and try to find more direct solution methods.

4.2.2 Cascade Mixing, Forthright Solutions.

The most direct way of solving the recoil mixing problem is to write a computer simulation code, supply it with reliable potentials or cross sections, and wait for output. As, however, $\sim 10^{18}$ projectiles/cm^2 are usually necessary to obtain a depth profile, the response time would be unacceptable if the individual ions and recoils were followed throughout their slowing down history. One can, though, solve this problem by injecting several ($\sim 10^{13}$ - 10^{14} cm^{-2}) ions at a time, as the profile changes caused by even such a high number of ions is still relatively small. In this way the individual ion and recoil trajectories are uninteresting and a statistical average picture is adequate; this leads to a discription within usual transport theory / 18, 29/ and the ballance equation (3.22) is then á relevant starting point for the calculation.

Quite extensive computer simulations have been performed within this scheme by Shimizu and coworkers /6/. A Monte-Carlo code was used to determine the relocation function $V_2(y',y'')$ for a pure target (the matrix, $k = 2$). Using now for any value of k

$$V_k(y',y'') = \frac{Q_k(y')}{N_o} V_2(y',y'') \qquad (4.20)$$

and inserting it into Eq. (3.19) and the bounded balance equation (3.25), the evolution of tracer profiles P_k ($k \neq 2$) was traced during irradiation. Equation (4.20) is strictly valid only for identical target constituents. The constant target density, which is a necessary condition for Eq.(3.25), was achieved by an implicite use of zero total relocation, $T = 0$; concerning the complications entailing from this assumption we refer to Sec. 3.3.1. Contrary to Sigmund and Gras-Marti /10,11/, however, sputtering was no external input quantity but a result of the simulation.

Obviously the V_k-functions obtained by computer simulation contain recoil relocation not only due to low energy cascade recoils, but also by high energy recoils with their anisotropic velocity spectrum. These latter ones were made reponsible for the shifts and asymmetric shapes of the apparent profiles found (surface density as a function of eroded depth). The asymmetry observed is, however, also found for isotropic cascade recoils alone (see below), and the shifts may well be due to the assumption of T = 0.

Instead of letting the relocation effect of $\sim 10^{14}$ projectiles be represented by the action of a single one, a computer simulation can be carried out where the relocation of $\sim 10^{14}$ target atoms are represented by the reaction of one single atom. This way of scaling down the problem to a handable size has been used in the simulations by Roush et al. /16/. Using a scaled target with relatively few atoms per unit volume their simulation code can - in principle - follow all details of the energy sharing, recoil generation and profile changes in complex targets. These authors clearly recognize the problem of target relaxation, and use exclusively the bounded system (3.1.2).

Here again the sputtering yield - and thus the speed of erosion - are not input parameters but result of the simulation of atomic relocations. The depth scale of the calculated external profiles thus contains no freely adjustable parameter.

There is no need for time-consuming Monte Carlo simulations, however, with their inherent opaqueness to understanding. All information for evaluation of the balance equation (3.22) for relocation by cascade recoils is available from analytic transport theory - at least in the representative cases (4.12), (4.14) and (4.15), and the Monte-Carlo simulation can be avoided. Littmark and Hofer /8,9/ based their evaluation entirely on such information and just used numerical methods to solve the balance equation. This allows the determination of non-linear as well as coupled systems. There is no need for additional approximations such as invoking diffusion analogies.

The functions needed for determining Eq. (4.12), and so to solve Eq. (3.22) in this approach, are F_E and F_{Rk}. Such functions have valuable scaling properties /18/ when they are determined on the basis of power cross sections, Eq. (2.2) :

$$F_E(E_1^0, \bar{e}_1^0, y) = N_o C_{12}(E_1^0)^{1-2m_{12}} f_E(y \cdot N_o C_{12}(E_1^0)^{-2m_{12}}, \bar{e}_1^0)$$

and

(4.21)

$$F_{Rk}(E_k, \bar{e}_k, y) = N_o C_{k2} E_k^{-2m_{k2}} f_R(y \cdot N_o \cdot C_{k2} E_k^{-2m_{k2}}, \bar{e}_k)$$

where f_E and f_R are normalized, dimensionless functions. This simplifies the evaluation of Eq. (4.12) but not the notation in the explicit expression for the ballance equation.

Introducing for brevity an effective local transfer function:

$$W_k(y',y) = f_k(Q_i(y')) F_E(y') \int \frac{1}{4\pi E_k^2} [F_{Rk}(y-y') - \delta(y-y')] dE_k d\bar{e}_k \qquad (4.22)$$

we obtain by inserting (4.12) in (3.17) and (3.19)

$$T_k(y) - S_k(y) = \int_0^\infty W_k(y',y) \frac{Q_k(y')}{N_o} dy' \qquad (4.23)$$

Using now $N_o = \sum Q_i$ we get for Eq. (3.22):

$$Q_k(\phi+d\phi, y+dy(\phi,y)) = Q_k(\phi,y) + dQ_k(\phi,y)$$

$$dQ_k(\phi,y) = \frac{d\phi}{N_o^2} \int_0^\infty \sum_{i=1}^K [Q_i(y)Q_k(y')W_k(y',y) - Q_i(y')Q_k(y)W_i(y',y)] dy'$$

$$+ \frac{d\phi}{N_o} F_{RI}(y) [N_o\delta_{1k} - Q_k(y)] \qquad (4.24)$$

$$dy(\phi,y) = \frac{d\phi}{N_o^2} \int_{y''=0}^y \left(\int_{y'=0}^\infty \sum_{i=1}^K [Q_i(y')W_i(y',y'')] dy' + N_o F_{RI}(y'') \right) dy''$$

The partial and total sputtering yields Y_k and Y are determined by the recoil relocation, and according to Eq. (3.23) we obtain:

$$Y = -\frac{1}{N_0} \int\limits_0^\infty \int\limits_0^\infty \sum_{i=1}^K \left[Q_i(y')W_i(y',y'') \right] dy' \, dy'' \qquad (4.25)$$

and finally:

$$Y_k = -\frac{1}{N_0} \int\limits_0^\infty \int\limits_0^\infty Q_k(y')W_k(y',y'') \, dy' \, dy'' \qquad (4.26)$$

Equation (4.24) evidently ⌐represents⌐ ∨ a non-linear coupled system of equations (even ⌐when⌐ disregarding Q-dependences in the W-functions). The dilute tracer approach (4.14) does not simplify Eq. (4.24) substantially. (Only in·the equal mass case (Eq. (4.15)) we can execute the summations as all $W_k = W$ are identical. We then obtain:

$$dQ_k(\phi,y) = \frac{d\phi}{N_0} \int\limits_0^\infty W(y',y) \left[Q_k(y')-Q_k(y) \right] dy' + \frac{d\phi}{N_0} F_{RI}(y) \left[N_0 \delta_{1k} - Q_k(y) \right]$$

$$(4.27)$$

$$dy(\phi,y) = \frac{d\phi}{N_0} \int\limits_{y''=0}^y \left(\int\limits_{y'=0}^\infty W(y',y'')dy' + F_{RI}(y'') \right) dy''$$

$$Y = - \int\limits_0^\infty \int\limits_0^\infty W(y',y'') \, dy' \, dy''$$

These equations have been derived in our previous communication /9/; they were presented, however, in the bounded target approach which, according to Eq. (3.9), is obtained by inserting $P_k(\phi,x) = Q_k(\phi, x-z(\phi))$ in Eq. (4.27) with $dz/d\phi = (Y-I_I)/N_0$.

The integro-differential equation systems, Eqs. (4.24 and (4.27) for the
evolution of the profiles Q_k can be solved in a stepwise manner.
The profiles are given and followed in a one dimensional depth
array (typical lattice-unit 1 Å). A small projectile-fluence dΦ ($\sim 10^{14}$ cm^{-2})
is injected and the profile changes calculated according to Eq. (4.24).
The new density values are not associated with the array depths y, but to the
shifted depths y + dy(ϕ,y). The density values at the array points are
therefore found by interpolation, and then the scheme is repeated.

In this way the internal distributions are traced as a function of flu-
ence ϕ or of eroded depth z . The important quantities for depth pro-
filing, namely the surface density $P_k(z,z)$ and the partial yield $Y_k(z)$, are
evaluated and stored in each step.

In Fig. 4 the evolution of a thin tracer in Si is shown, calculated in
the equal mass approach (4.27). Fig. 4A shows the profile development due
to bombardment with 2 keV Ne$^+$ ions. These ions are not collected in the
target to a substantial degree and have been neglected in the calculation.
Between the curves shown, the surface has been eroded by 20 Å. An in-
creasing asymmetric smearing of the original profile is observed, covering
finally the entire cascade region. This being loosely defined by the F_E-
function, which is also indicated in Fig. 4A.

Inclusion of the implanted ions causes much faster smearing of the inter-
nal profiles, when followed as a function of eroded depth. This can be
observed in Fig. 4B . where the development of the same system as in Fig. 4A

is shown, now depth profiled with 2 keV O^+ ions. Distributions are here

shown for each 10 $\overset{o}{A}$ eroded. F_E and F_{RI} are also indicated.

The surface concentration and the relative partial yield in the two above

cases are shown in Fig. 4C, as a function of eroded depth. Firstly we ob-

serve the dramatic smearing of the original profile. The apparent profiles

have *widths comparable to the cascade dimensions*, and are further *strongly*

asymmetric. This makes *any definition of broadening by a single number im-*

possible. One has to compare experimental results with the calculated

,entire,
⌄ profiles in order to judge on the validity of the theoretical approach

/30/. For a more detailed discussion of external profiles originating from

thin tracer layers at different original depths see Ref. /9/.

The second effect seen in Fig. 4C is that there is a slight *difference*

between the corresponding surface-value- and partial-yield profiles.

This is due to the finite depth of origin for sputtered particles /9/.

The third observation from Fig. 4C is the *strong influence by the collection*

of injected ions in the target. If the implanted ions can be neglected (Ne^+),

the mean depth of the apparent profiles is almost identical to the position

of the original distribution. Inclusion of the implanted ions (O^+) means that

larger fluences are needed (for the same sputtering yield Y) for eroding down

to a certain depth. This should result in larger broadening relative to the

case where the ion collection is neglected. The injected ions are, however,

in the average implanted at depths larger than those where they cause recoil

,entire, ,seems to be,
generation, so that the⌄profile ⌄ pressed towards the surface. For sputter-

ing yields close to 1 this latter effect may dominate so that even the broad-

ening becomes less than in the case where the implanted ions are neglected.

Fig. 4C is in this respect an extreme example. With a sputtering yield Y=1.1

and an implantation probability I_I= .93 we need 6-7 times as many O^+ ions as

Ne^+ ions to erode down to the same depth.

In order to illustrate the effect of the implanted ions on the depth- and fluence scales we consider a simplified example where we follow markers in the target without letting these be exposed to mixing. We can describe their position below the target surface by Eq. (3.22) with $T = 0$ then.
Assuming that the erosion is simply a cutting off of surface layers and using the simplified box-shaped implantation profile

$$F_{RI}(y) = \begin{cases} I_I/R & o < y < R \\ o & R < y \end{cases} \qquad (4.28)$$

we obtain   from Eq.(3.22) with (3.18) inserted :

$$dy(\Phi,y) = \frac{d\Phi}{N_0} \begin{cases} I_I\, y/R - Y & o < y < R \\ I_I - Y & R < y \end{cases} \qquad (4.29)$$

This equation can easily be solved to yield the fluence $\phi(x_0)$ needed to bring the original marker position $y = x_0$ to the surface. This quantity is shown in the top part of Fig. 5 for different values of x_0 and the parameter $\beta = Y/(Y-I_I)$. $\beta = 1$ corresponds to neglection of the implanted projectiles or to an extreemely high sputtering yield $Y \gg I_I \sim 1$. Accordingly increasing values of β correspond to sputtering yields decreasing towards I_I.

For deep lying markers ($x_0 > R$) the required fluence increases strongly with the value of β, i.e. with decreasing sputtering yield ($Y \rightarrow I_I$). This is a consequence of erosion being increasingly a removal of already implanted projectile atoms. In the implantation region ($0 < x_0 < R$) ,however, the dependence on β is seen slowly to disappear, so that the speed of motion of the marker, $dx_0/d\phi$, here becomes almost independent of β. Since recoil mixing is concentrated to this region, one expects profile broadening to be relatively unaffected by the value of β too. Concluding, the inclusion of implanted projectiles for sputtering yields around unity will result in increased fluences for depth profiling, but will hardly influence the profile shape as long as a comparison is made on a fluence scale. The situation is, however, quite different in an eroded-depth-scale. The bottom part of Fig. 5 shows the actual depth $z(x_0)$ eroded in the target when a certain marker depth x_0 is seen at the surface: $z(x_0) = (Y-I_I)/N_0 \cdot \phi(x_0)$, where $\phi(x_0)$ is taken from the top part of Fig. 5. Obviously, the marker speed dx_0/dz is unity for $x_0 > R$, but, because of implantation behind the marker in the region $o < x_0 < R$ (for $\beta \neq 1$), the speed is drastically increased here. All depths will then appear earlier at the surface for $\beta \neq 1$, i.e. when the implanted projectiles are taken into account. This means that in an eroded-depth-scale (such as in Fig. 4C) the apparent profile seems to be both compressed and shifted towards the surface for large β.

The results of Fig. 5 and Fig. 4c urge care when comparing experimental shifts and broadenings mutually or with theory. Thus, in addition to the well known problems in converting an experimental fluence-scale into a depth-scale, the interacting role of implanted projectiles represent a severe complication.

The reason for the low relative intensity of the apparent profile for O^+ bombardment in Fig. 4C is the pile up of O-atoms in the target. In the steady state the surface concentration as well as the sputtering yield will consist of I_I/Y ($\sim$85%) implanted ions /23/. In this respect the example of O^+ may not be too physically realistic.

O^+ does not really mean Oxygen here, the O^+-profiles can as well be interpreted as if obtained by Si-selfion-bombardment. O^+ was merely chosen because it is an often used projectile species in SIMS and because it is - contrary to inert gas ions (Ne^+) - accumulated in most samples. Although consistent in this presentation, this example demonstrates that effects like preferential sputtering, solid solubility limits, and phase-transformation must be taken into account in realistic descriptions.

5. Summary and Outlook

In the preceeding review, the various models and theoretical approaches pro-
posed for calculations of the alteration of concentration profiles upon ener-
getic particle bombardment have been discussed. In order to allow comparison
of these widely diffening models they were presented within a unified scheme.
This scheme was based on a general balance equation and guided by existing
solutions to the recoil mixing problem, applying the concept of transport
theory of atomic collision cascades in amorphous solids. In addition, a path
was shown how thermally activated mixing processes can be included. This im-
portant aspect was not elaborated, however, since it requires substantially
more information on the specific metallurgy of the samples in question. And,
furthermore, this article was intended to review collisional mixing. It pre-
dominately concentrates on profile deformation as it appears in in-depth con-
centration profiling by sputter etching. It demonstrates that the often made
assumption of a congruent transformation of internal concentration distribu-
tions to external so-called sputter-profiles is seriously incorrect. Although
the calculation of the evalution of internal profiles will always be the first
step in determining sputter profiles, the next one must take into account the
gradual deformation as the profile passes through the surface. It appears,
that a random walk treatment is not too bad an approximation for (internal)
concentration distributions, but it is unacceptable for sputter profiles.
Moreover, this latter transformation causes pronounced asymmetries, the degree
of skewness depending on the relative speeds of erosion and relocation. Thus,
without back-transforming measured sputter-profiles into internal concentra-
tion distributions it is impossible to quantify, for instance, the contribu-
tion of primary recoils to profile deformation - an often assumed reason for

asymmetric profiles. In fact detailed studies have made clear that profile adulteration under conditions typical of sputter-profiling is mostly due to cascade recoils, while primary recoils have generally only a small influence.

Recoil mixing is, of course, not the only reason for alteration of genuine concentration distributions in solids subjected to energetic particle bombardment. In the authors opinion, however, this collisional component of atomic mixing is now theoretically well under control: any given profile can be traced both inside the solid and when it appears at the surface, isotropic as well as anisotropic cascades can be dealt with, recoil implantation and projectile accumulation can be included when it deems necessary; the assumption of equal masses of matrix and tracer atoms has recently been found to be even less restrictive as estimated previously. If, on the other hand, this assumption can no longer be accepted dilute-tracer-calculations allow at least estimates. Both analytical treatments and Monte-Carlo simulation codes are at hand, so that it appears possible now to extract from measured distribution functions the collisional component in order to unravel chemical-, thermodynamic, and electrostatic drift components to atomic mixing.

Further improvements can, on the other hand, be obtained with more realistic collision cross sections, a more refined sputtering model with an explicite ejection threshold, and with an atomistic interpretation for density relaxation in high fluence irradiation (e.g. interstitial diffusion?). But at present more important in sputter profiling seems to be to clear the situation faced with projectile accumulation. Such projectiles are - for reasons other than mixing - often preferred to inert gas ions; their presence in the target complicate the situation significantly. It does not seem to be possible to

achieve good agreement with experimental results without taking into account the actual multiple phase situation and include on this basis preferential ejection in the sputtering model.

Although this review concentrates on low-energy atomic mixing, it is finally worthwhile to draw attention to the large experimental efforts, which are at present devoted to high energy mixing. The interpretation of such experiments is in many respects simpler: relative low fluences are sufficient to obtain measurable profile alteration and the complications due to internal external-profile transformation do not exist, because the internal profiles can be studied directly by well established non-destructive depth analysis methods (e.g. RBS). Experiments have demonstrated sofar that phenomena like solid solubility, phase transformation, migration and thermal and radiation enhanced diffusion may play a dominant role in ion beam mixing, depending, of course, strongly on the system studied. Even then, however, recoil mixing, as an inherent effect, is important: it constitutes the non-circumventable alteration of concentration distributions in solids under energetic particle irradiation, or, in ion-beam processing of materials, the minimum achievable compositional modification.

6. List of symbols

The following is a list of the symbols used throughout this paper. Locally introduced and applied symbols are not included. The subscript indicating the atomic species under consideration (k) is sporadically omitted in Sect. 1 and 2 when otherwise subscripted quantities are unambiguously obvious.

a_k Mean depth of k-tracer distribution [$\overset{\circ}{A}$]

A_k Number of k-atoms in tracer distribution [atoms/$\overset{\circ}{A}{}^2$]

D Diffusion coefficient [$\overset{\circ}{A}{}^2$/sec]

$\bar{e}_k$, $\bar{e}_1^o$ Direction of motion of a k-recoil-atom [unit vektor]. Superscript o indicating original projectile direction.

E_k, E_1^o Kinetic energy of a k-recoil-atom [keV]. Superscript o indicating original projectile energy.

E_d Threshold energy for a permanent displacement [keV]

f_k Energy sharing factor

F_E Deposited energy depth distribution [keV/$\overset{\circ}{A}$]

F_{RI} Projectile range distribution [atoms/$\overset{\circ}{A}$]

F_{Rk} k-recoil range distribution [atoms/$\overset{\circ}{A}$]

$\bar{F}_p$ Deposited momentum depth distribution [(keV·amu)$^{1/2}$/$\overset{\circ}{A}$]

F_{Vk} Depth distribution of k-recoil velocity spectrum [atoms/($\overset{\circ}{A}$ · keV · steradian)]

Φ Projectile fluence [atoms/$\overset{\circ}{A}{}^2$]

$\dot{\Phi}$ Projectile flux-density [atoms/($\overset{\circ}{A}{}^2$· sec)]

γ_{ik} Maximum relative energy transfer in a collision between an i-atom and a resting k-atom.

Γ Diffusional jump frequency [sec^{-1}]

I_I Projectile implantation probability

I_k Recoil intensity function, i.e. the total number of generated k-recoil-atoms [atoms/$\overset{\circ}{A}$] at a given depth.

J_k Normalized velocity spectrum of generated k-recoil-atoms [atoms/(keV · steradian)]

I_k, J_k are used in situations where the depth dependence of F_{Vk} can be split off into a separate function.

k Atomic species number. k=1: projectile, k≧1 target atoms (as a standard k=2 denotes target matrix and k≧3 tracer atoms).

K	Number of considered atomic species.
κ	Dynamically dominant atomic species.
m_{ik}	Power-parameter in scattering cross section for the interaction of an i-atom with a resting k-atom.
M_k	Mass of k-atom [amu]
N	Target number density [atom/$\mathring{A}^3$]
N_0	Target number density, standard value.[atoms/$\mathring{A}^3$]
P_k	Concentration depth profile of k-atoms [atoms/$\mathring{A}^3$]
Q_k	Auxiliary concentration depth profile of k-atoms [atoms/$\mathring{A}^3$]
R_I	Projectile reflection coefficient.
$\bar{R}$	Average diffusion step-length [$\mathring{A}$](mean projected range of recoils).
S_k	Depth differential sputtering yield of k-atoms [atoms/(projectile·$\mathring{A}$)]
$d\sigma_{ik}$	Differential scattering cross section for the interaction of an i-atom with a resting k-atom [$\mathring{A}^2$]
σ_k	Standard deviation of k-tracer distribution [$\mathring{A}$]
T_k	Effective total transfer function (yield) of k-atoms. [atoms/(projectile·$\mathring{A}$)]
U_k	Relative relocation function (yield) of k-atoms. [atoms/(projectile· unit target density ·$\mathring{A}^2$)]
V_k	Absolute relocation function (yield) of k-atoms [atoms/(projectile·$\mathring{A}^2$)]
W_k	Effective local transfer function (yield) of k-atoms [atoms/(projectile·$\mathring{A}^2$)]

x	Depth in target, measured perpendicular to the surface from its original position [$\overset{o}{A}$]
y	Depth in target (auxilliary), measured perpendicular to the surface from its actual position [$\overset{o}{A}$]
Y	Total sputtering or erosion yield [atoms/projectile]
Y_k	Partial sputtering or erosion yield of k-atoms [atoms/projectile]
Y_{PR}	Yield of implanted primary recoils [atoms/projectile]
z	Eroded depth (under the assumption of a target density N_o) [$\overset{o}{A}$]
Z_k	Atomic number of k-atoms.
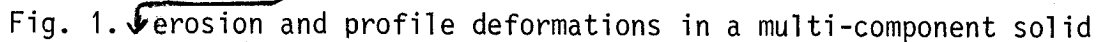
7. References

/1/ R.S. Nelson, Radiat. Eff. $\underline{2}$ (1969) 47

/2/ J.G. Perkins and P.T. Stroud, Nucl. Instr. Meth. $\underline{102}$ (1972) 109

/3/ R.A. Moline, G.W. Reutlinger and J.C. North, in Atomic Collisions in Solids, Eds. S. Datz et al.; Plenum Press 1976, Vol. 1, p. 159.

/4/ R. Kelly and J. Sanders, Surface Sci. $\underline{57}$ (1976) 143

/5/ S. Dzioba and R. Kelly, J. Nucl. Mater. $\underline{76}$ (1978) 175

/6/ T. Ishitani and R. Shimizu, Appl. Phys. $\underline{6}$ (1975) 241

R. Shimizu, Proc. 7th Int. Vac. Cong. & 3rd Int. Conf. Solid Surf. Vienna 1977, p. 1417

S.T. Kang, R. Shimizu and T. Okutani, Jap. Appl. Phys. $\underline{18}$ (1979) 1987

/7/ H.H. Andersen, Appl. Phys. $\underline{18}$ (1979) 131

/8/ W.O. Hofer and U. Littmark, Phys. Lett. $\underline{71A}$ (1979) 457

/9/ U. Littmark and W.O. Hofer, Proc. 4th Int. Conf. Ion Beam Analysis, Aarhus, Denmark, 1979, published in Nucl. Instr. Meth $\underline{168}$ (1980) 329

/10/ P. Sigmund and A. Gras-Marti, ibid. 389

/11/ P. Sigmund and A. Gras-Marti, Proc. 2nd Int. Conf. Ion Beam Modification of Materials Albany, New York, 1980, published in Nucl. Instr. Meth. $\underline{182/183}$ (1981) 25

A. Gras-Marti and P. Sigmund, Proc. Symposium on Sputtering, Techn. Univers. Wien, April 1980, p. 512, Eds.: P. Varga, G. Betz, F.P. Viehböck; also published in Nucl. Instr. Meth. $\underline{180}$ (1981) 211

/12/ P.K. Haff and Z.E. Switkowski, J. Appl. Phys. $\underline{48}$ (1977) 3383.

/13/ G. Carter, D.G. Armour, D.C. Ingram, R. Webb, and R. Newcombe, Radiat. Eff. Lett. $\underline{43}$ (1979) 233

/14/ S. Matteson, Appl. Phys. Lett. $\underline{39}$ (1981) 288

S. Matteson, B.M. Paine, M.G. Grimaldi, G. Mezey and M.-A. Nicolet, Proc. 2nd Int. Conf. Ion Beam Modification of Materials, Albany, New York 1980; published in Nucl. Instr. Meth. $\underline{182/183}$(1981) 43

/15/ Z.L. Liau, B.Y. Tsaur and J.W. Mayer, J.Vac.Sci. Technol. $\underline{16}$ (1979) 121

/16/ M.L. Roush, T.D. Andreadis, F. Davarya and D.F. Goktepe,
Proc. 5th Int. Conf. Ion Beam Analysis, Sydney 1981. published in
Nucl. Instr. Meth. 191 (1981) 135

M.L. Roush, T.D. Andreadis and O.F. Goktepe, Radiat. Eff. 55 (1981) 119

/17/ J. Lindhard, V. Nielsen and M. Scharff, Mat. Fys. Medd., Dan.Vid. Selsk. 36
No. 10 (1968)

/18/ K.B. Winterbon, P. Sigmund and J.B. Sanders, ibid. 37, No. 14 (1970)

/19/ S. Hofmann, Appl. Phys. 9 (1976) 59 and 13 (1977) 205

J. Erlewein and S. Hofmann, Thin. Sol. Films 69 (1980) L39

H. Oechsner and A. Wucher, Applicat. Surface Sci., 10 (1982) 342

/20/ A. Benninghoven, Z. Physik 230 (1971) 403

/21/ K. Wittmaack and F. Schulz, Thin. Sol. Films 52 (1978) 259
J. Kirschner and H.W. Etzkorn, this volume.

/22/ N.O. Andersen and P. Sigmund, Mat. Fys. Medd. Dan. Vid. Selsk. 39 no. 3
(1974)

/23/ U. Littmark and W.O. Hofer, Nucl. Instr. Meth. 170 (1980) 177

/24/ P. Sigmund, Appl. Phys. Lett. 14 (1969) 114

/25/ U. Littmark and A. Gras-Marti, Appl. Phys. 16, 247 (1978)

S. Fedder and U. Littmark, J. Appl. Phys., 194 (1982) 607

/26/ M.T. Robinson, Phil. Mag. 12, 145 (1965), ibid 12 741 (1965), ibid 17,
639 (1968)

/27/ J.B. Sanders, Thesis, University of Leiden (1968)

/28/ U. Littmark and P. Sigmund, J. Phys. D 8, 241 (1975)

/29/ J. Lindhard, V. Nielsen, M. Scharff and P.V. Thomsen, Mat. Fys. Medd. Dan. Vid.
Selsk. 33, no. 10 (1963)

/30/ H.W. Etzkorn, U. Littmark and J. Kirschner, Proc. Symposium on Sputtering,
Techn. Univers. Wien, April 1980, p. 542,
Eds.: P. Varga, G. Betz, F.P. Viehböck

/31/ H.E. Roosendaal, J.B. Sanders and U. Littmark, Phys.Rev. B26 5261 (1982).

/32/ W.O. Hofer and U. Littmark, in Proc. 3rd Int. Conf. on Secondary Ion Mass
Spectrometry, Budapest 1981,
Eds.: A. Benninghoven, J. Giber et al. p. 201, Springer-Verlag, Berlin,
Heidelberg, New York 1982

8. <u>Figure Captions</u>

Schematic

Fig. 1. Erosion and profile deformations in a multi-component solid

during bombardment with ions of energy E_i^o. The description of the profiles, $Q(y)$ and $P(x)$, are defined in the text.

(A) Shows the original target, at fluence $\Phi= 0$.

Compositional changes in an interval around depth y is due to

atoms leaving this interval, and due to moving atoms generated

in other depth intervals (around y') which are slowed down to

rest at y. The depth dependence of the generation - probability

for such atoms, F_E, is indicated.

(B) Shows the auxiliary Q-y target system with constant total den-

sity N_o, in which profile changes are calculated basically. This

system has a well-defined surface which is located at y= o at

all fluences. The distorted profile is indicated together with

F_E.

P-x

(C) and (D) show two examples of "real" target models :

(C) the bounded system,which has a well defined surface positioned at a depth

x= z(Φ) (the eroded depth) and a constant total density, and

(D) the unbounded system, where a surface can not be defined.

In both cases the distorted profile and F_E is indicated. These

are obtained by a transformation of the auxilliary system which

is specific for the "real" target model. For Φ= o all shown

systems are identical with (A).

Fig. 2   Mean depth, standard deviation and skewness of

internal impurity profile during diffusive mixing

with depth dependent diffusion coefficient:

$$D_k(y) = \frac{\alpha}{z} \frac{dz}{dt} (R^2 - (y-m)^2)/R$$

(Eqs.(3.36) and (3.39))

$m = \frac{2}{3} R$ has been used and the original profile has:

$a_k = \frac{5}{3} R$, $\sigma_k = \frac{1}{20} R$ and zero skewness.

The solution to (3.40) is shown full drawn, together

with the gaussian-approach (3.33) in which $a_k = o$ and

skewness$= o$.

Three different values of α are used. For the systems

shown in Fig. 4 $\alpha = 0.3$ would be representative.

Fig. 3   Transformation of internal gaussian profiles to surface

concentration profile.

$$P_k(z,x) = \frac{N_o}{\sqrt{2\pi\sigma_k^2}} \exp\left(- \frac{(z-a_k)^2}{2\sigma k^2} \right)$$

where $\sigma_k = \sigma_k(z) = (z/a_k)^p \cdot 80 \, \mathring{A}$

and $a_k = 200 \, \mathring{A}$ have been chosen to approximate the

situation in Fig. 4. $p = 1/2$ correspond to usual

thermal diffusion, whereas $p = 1-2$ correspond to

radiation enhanced diffusion or collisional reloca-

tion. Observe: the internal profiles are symmetric,

whereas the surface concentration shows prounounced

tailing behaviour.

Fig. 4.   The evolution of a thin tracer (A and B) (originally positioned

at large depth in the target) and apparent profiles (C)

(surface concentration and relative partial yield) as

a function of eroded depth z.

In Figure 4A (2 keV $Ne^+ \to Si$) the implanted ions are dis-

regarded whereas in Figure 4B (2 keV $O^+ \to Si$) the collec-

tion of ions on the target is taken into account. The

scheme of Littmark and Hofer /9/ has been used for the

calculation, i.e. the assumption being that O, Ne and

Si have identical dynamics in the Si target. The tracer

is essentially Si, or an element not to far from Si on

the periodic table.

Fig. 5.   Fluence Φ and eroded depth z needed to bring a marker

to the surface by simple erosion and implantation

according to Eq.(4.28).

Mixing of the marker has been neglected. Different

values for $\beta = Y/(Y-I_I)$ has been used. $\beta = 1$ is valid

if implantation can be neglected. $\beta = 6$ is representative

for the case shown in Fig. 4 , to which this figure is an
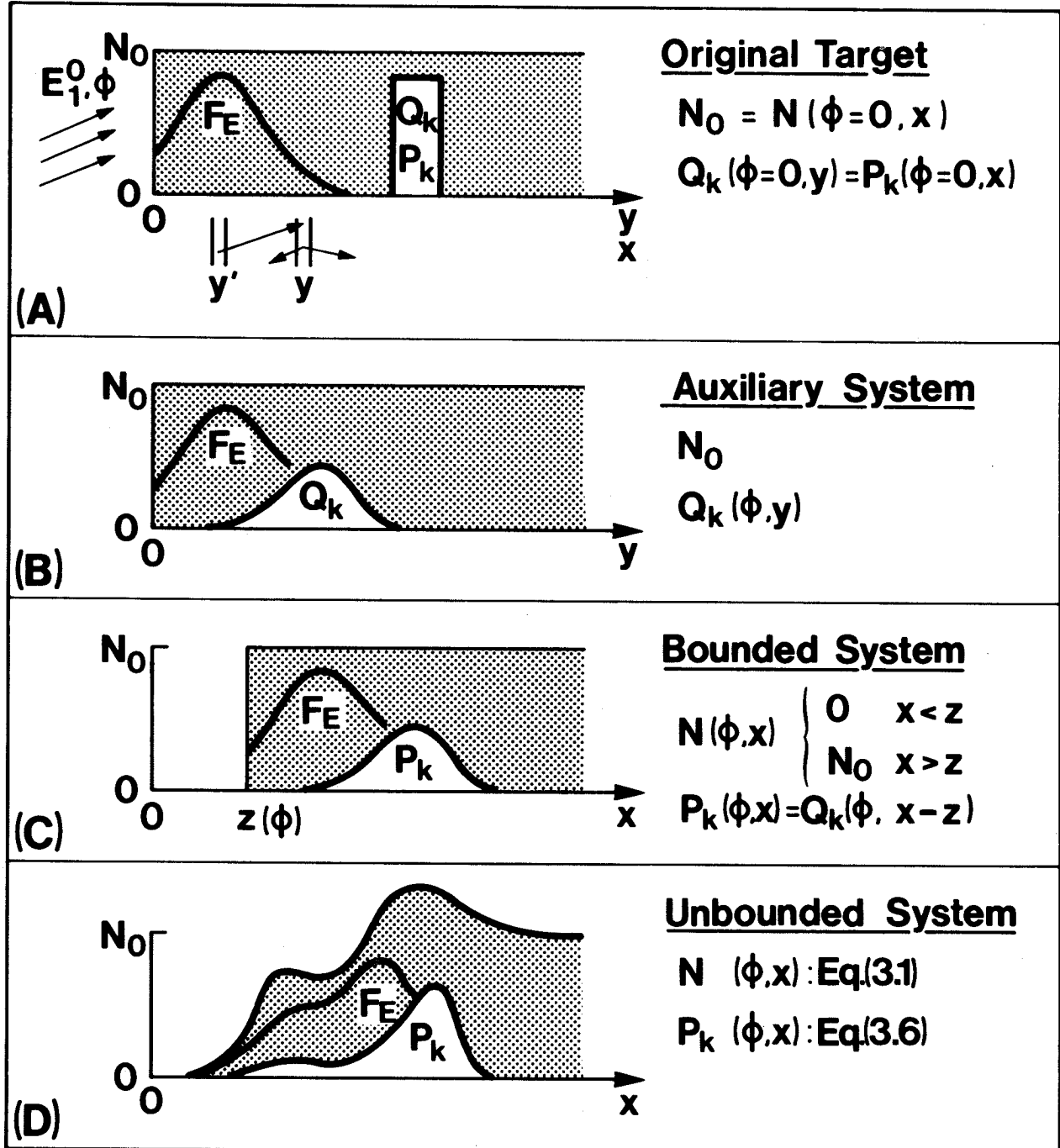
ancillary plot.

9. Figures.

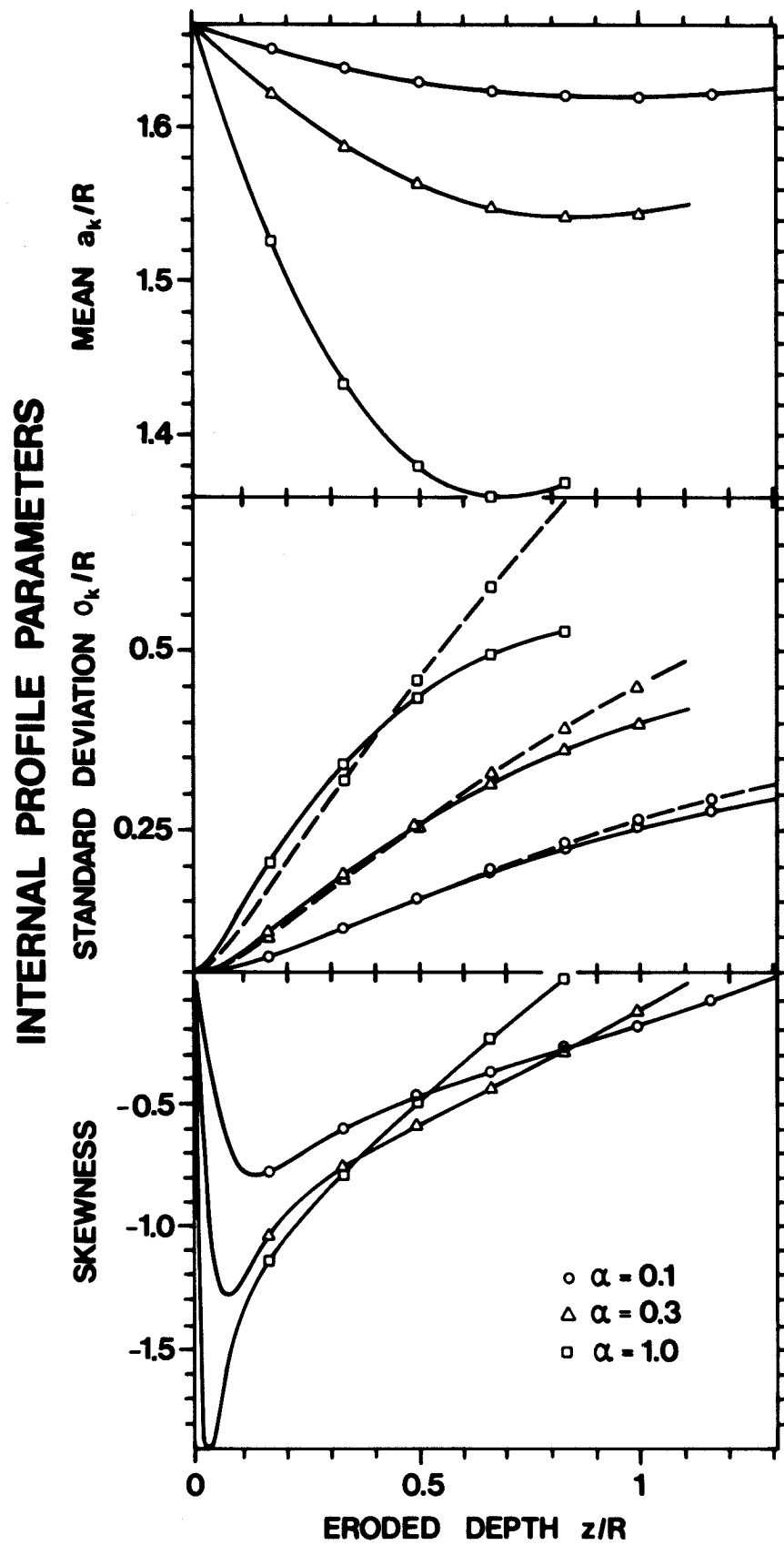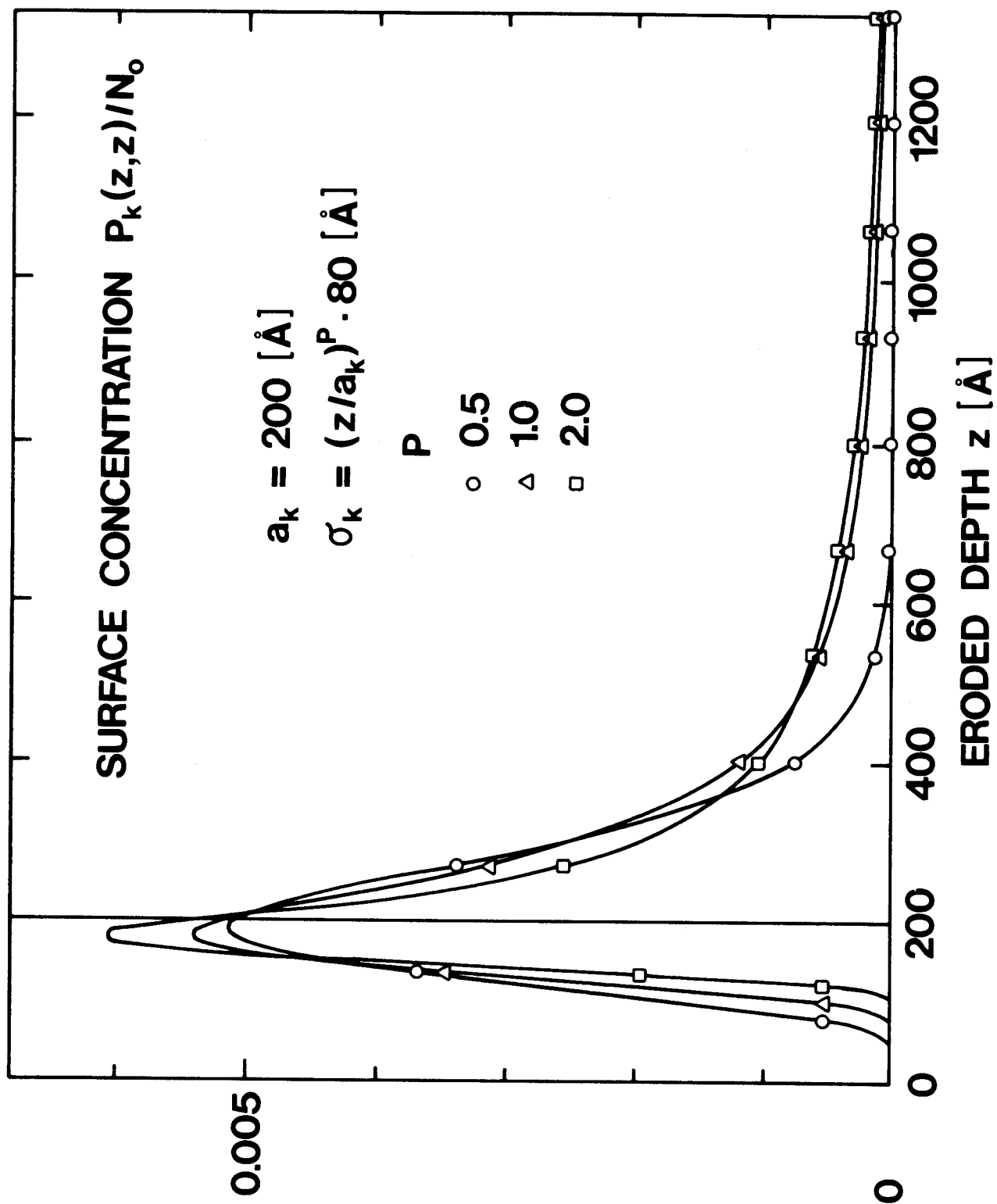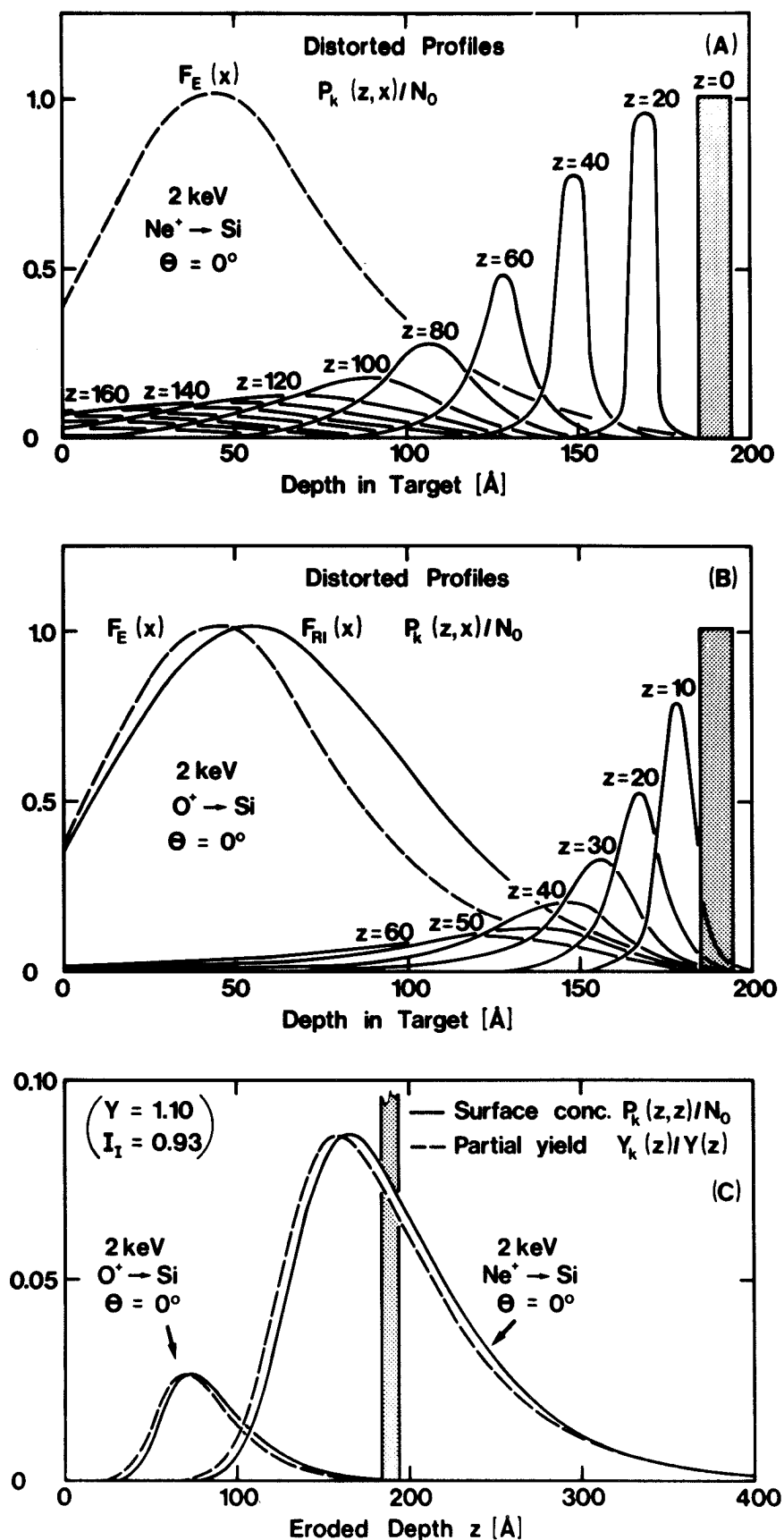**(A)** $E^0_{1,\phi}$ N_0 F_E Q_k P_k O y' y y x

Original Target

$N_0 = N(\phi=0,x)$

$Q_k(\phi=0,y)=P_k(\phi=0,x)$

(B) N_0 F_E Q_k O y

Auxiliary System

N_0

$Q_k(\phi,y)$

(C) N_0 F_E P_k O $z(\phi)$ x

Bounded System

$N(\phi,x)\begin{cases} 0 & x<z \\ N_0 & x>z \end{cases}$

$P_k(\phi,x)=Q_k(\phi, x-z)$

(D) N_0 F_E P_k O x

Unbounded System

$N\ (\phi,x): Eq.(3.1)$

$P_k\ (\phi,x): Eq.(3.6)$

Fig. 1.

Fig. 2

Fig. 3

Fig. 4

Fig. 5